COMPUTATIONAL MODEL FOR TRANSIENT AND STEADY STATE ANALYSIS OF A 1-DIMENSIONAL AUTO-THERMAL REFORMER

by

SRIKANTH HONAVARA-PRASAD

Presented to the Faculty of the Graduate School of

The University of Texas at Arlington in Partial Fulfillment

of the Requirements

for the Degree of

MASTER OF SCIENCE IN MECHANICAL ENGINEERING

THE UNIVERSITY OF TEXAS AT ARLINGTON

DECEMBER 2010

Copyright © by Srikanth Honavara-Prasad 2010

All Rights Reserved

ACKNOWLEDGEMENTS

A blissfully ignorant boy once walked into the office of a fuel cell expert and told him that he wanted to work on something that would help alleviate Global Warming. The professor laughed but gave the boy an opportunity to prove his worth. This is the story of me and Dr. Daejong Kim. It is a sad feeling to part because he is my first mentor. I take this opportunity to sincerely thank him for all the financial support and moral encouragement that he bestowed upon me during the course of my MS.

I would like to specially thank Dr. Albert Tong and Dr. Fuqiang Liu for their time and effort in being a part of my thesis committee.

I am deeply indebted to my family, my mother K.R. Gayathri, father Dr. H.V Prasad, sister Sushma and brother-in-law Girish for always believing in me and being my support structures. The course of my life would have been very different if not for the persistence of my father and sister who were instrumental in seeing me through my MS. I will forever be grateful to my mother for calling me every single day and being the “best-est” mother on this planet.

In a distant land, friends are family. Heartfelt thanks and gratitude goes out to all my friends for all the wonderful times. I would specially like to thank Mamata who created a whole new dimension to the word “trust”. Finally, I would like to thank all the members in my lab that made my stay at “The Micro-turbo-machinery and Energy Systems Laboratory” a memorable one.

December 22, 2010

ABSTRACT

COMPUTATIONAL MODEL FOR TRANSIENT AND STEADY
STATE ANALYSIS OF A 1-DIMENSIONAL
AUTO-THERMAL REFORMER

Srikanth Honavara-Prasad, M.S
The University of Texas at Arlington, 2010

Supervising Professor: Daejong Kim

This study presents a 1-dimensional mathematical model of steam reformer to be used with high temperature solid oxide fuel cell (SOFC). Steam reforming (SR) is widely used in industries to produce hydrogen from hydrocarbons. There are various physical processes associated with chemical reactions in the SR of methane such as mass, heat and momentum transport. In this study a one-dimensional SR reactor with built-in preheater and mixing chamber connected to fuel gas and steam reservoirs is modeled and analyzed. The main part of the reformer is a metallic tube with catalyst coating on the inner walls, and it can be modeled as a one-dimensional flow channel. The transient continuity, flow momentum and energy equations are applied for discretized control volumes along the flow channels and the energy equation is applied to the tube wall with appropriate heat transfer model. The preheater is modeled as part of the tube without catalyst coating. The mixing chamber is modeled as an adiabatic control volume and transient mass continuity and energy equations are applied to find gas pressure and temperature in the mixing chamber. All transient governing equations are solved using a time-marching technique to simulate the transient thermal dynamics and concentration profiles within the reformer, preheater and mixing chamber. In addition, steam to carbon ratio at the mixing

chamber is calculated and used as a numerical control parameter to achieve required fuel and steam reservoir pressures. Results in terms of local temperature and reformate composition are discussed for different prescribed reformer wall temperatures for various pressure gradients along the flow direction.

The developed preliminary SR model is extended to Auto-Thermal Reformer (ATR) by introducing controlled flow of air into the reactor leading to combustion within the mixing chamber and the tube. The ATR operates at high temperatures due to combustion and hence the need for preheater and external heating source is eliminated. The developed computational model provides a very effective simulation tool for optimizing reformer design.

TABLE OF CONTENTS

LIST OF ILLUSTRATIONS

Figure Page

LIST OF TABLES

Table Page

CHAPTER 1

INTRODUCTION

1.1 Background

The fruits of industrialization are pollution and population explosion. Never before in our history did we have 6.5 Billion people living on this planet. As Dr. Bartlett put forth [1] “The greatest shortcoming of the human race is our inability to understand the exponential function”. The human population explosion (Figure 1.1) [2], our resource consumption (Figure 1.2) [3] and the pollution we are causing have been exponential and we are doing little to mitigate the dangerous problems we might face if we continue to tread the path.

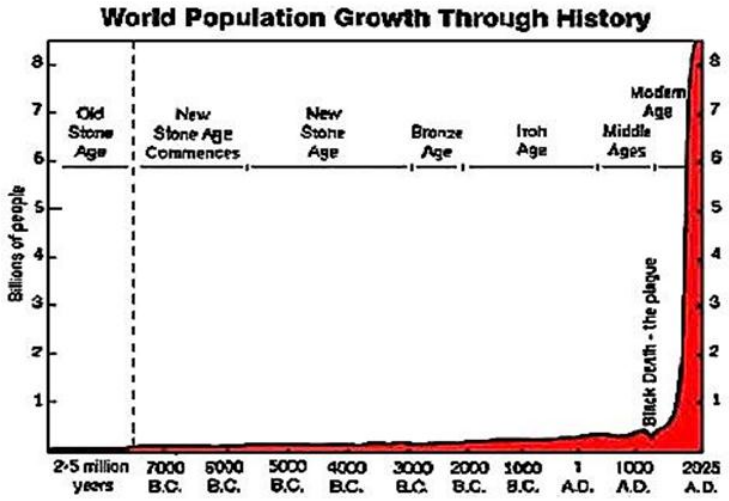

Figure 1.1 Population growth through time

As developing countries are adopting the western model of industrialization, it is becoming increasingly difficult to meet the demands for energy. Fossil fuels are the primary sources of energy in most industries. There are some industries that simply cannot sustain without them.

One of the most important fossil fuels that propelled growth like none other was oil. The automobile industry of the 20th century was based on the construct that oil would be available in plenty.

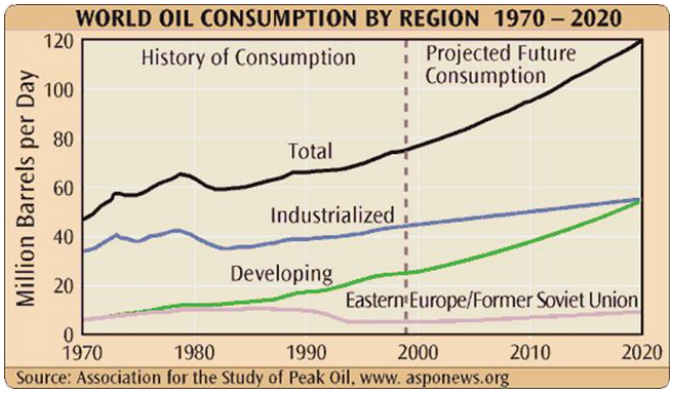

Figure 1.2 World oil consumption and estimates

In 1974, geoscientist M. K. Hubbert predicted that the oil production would peak by the end of the century. According to Dr. Colin Campbell of Association for the Study of Peak Oil (ASPO) [4], “The term peak oil refers to the maximum rate of oil production in any area under consideration, recognizing that it is a finite natural resource, subject to depletion.”

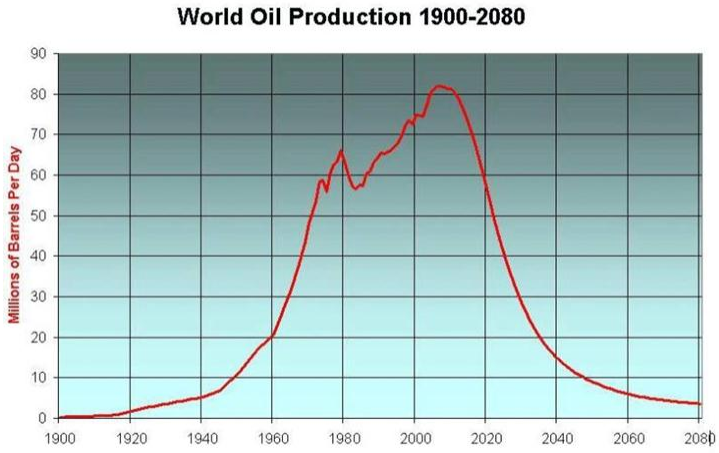

Figure 1.3 World oil production and estimates

It is now widely believed that oil production will start declining while the demand for it will continue to increase which could lead to unfathomable social complications since our lifestyle revolves around the usage of oil.

The Hubbert diagram in Figure 1.3 indicates the world oil production chronologically and makes prediction for the future of oil production [5]. The prediction is based on observed trends in many oil producing countries that have already attained peak production and now the production is in decline phase. The Hubbert's curve holds good for most of the cheap finite natural resources in a market economy. This means that resources such as coal or natural gas which we assume to be in large reserves will be depleted in a similar fashion.

The mechanisms leading to the bell-shaped curve are well understood. An abundant cheap resource that is extracted leads to economic growth and future investments. However, with time the resources get depleted and there is an increase in production cost owing to extraction from lower quality reserves. Ultimately there comes a time when the production costs become exorbitant leading to reduced investments and in turn reduced production [6].

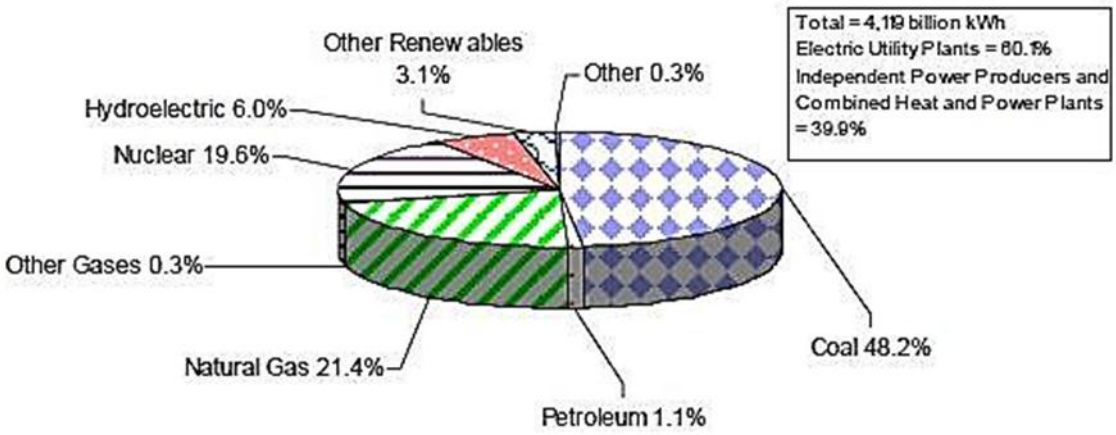

Figure 1.4 Sources of electricity in the USA

One look at the “Electricity” industry is enough to give us insight into our addiction to fossil fuels. According to the Department of Energy (DOE), 70% of the electrical power generated in 2008 came from fossil fuels [7].

We can observe from Figure 1.4 that coal still stands out as the base power source in USA since it meets almost half of the entire demand. Though large deposits of coal exist, harnessing electrical power from coal comes at the cost of environmental degradation. This is because coal is largely used as a solid fuel and is utilized by its combustion to generate steam in large boilers and drive turbines to produce electric power. New methods such as coal gasification for the production of syngas which can be used as an alternative fuel are being used in many places but this still doesn’t curb the toxic emissions. In fact, major concern when utilizing coal is the traces of mercury that exists in coal which on combustion leads to toxic compounds that are highly carcinogenic [8].

Nuclear energy accounts for almost 20 percent of the net electricity produced. Though this energy resource is reliable, the environmental effects are of grave concern since the radioactive wastes are hard to dispose. In fact, dumping radioactive wastes in landfills makes the land totally useless for any other purpose. Thus, there are many critics against the use of nuclear energy. Hydro-electric power plants are known to cause ecological imbalances and form only minor chunk of our electricity production. This means that fossil fuels will still remain the primary source of our electrical energy.

Since fossil fuels cannot last forever and the effects of climate change are irreversible, transition to clean and renewable sources of energy is gaining momentum at least in research laboratories. Apart from solar power panels, wind farms and bio-fuels, major technological advancements are taking place in the areas of fuel cells. Hydrogen has been recognized as one of the most important energy carriers during this transition period due to its high efficiency and low pollution. Also, the Department of Energy’s (DOE) initiative to promote hydrogen fuel

cells has propelled the research interest in hydrogen production, storage and distribution systems.

1.2 Reforming Basics

Hydrogen is the most abundant gas in the world making up almost 90% of the atoms in our universe. Its contribution by weight is accepted to be around 70% [9]. Though it is so abundant, due to its high reactivity, it combines with most elements to form compounds. So, hydrogen production involves removal of hydrogen from its compounds.

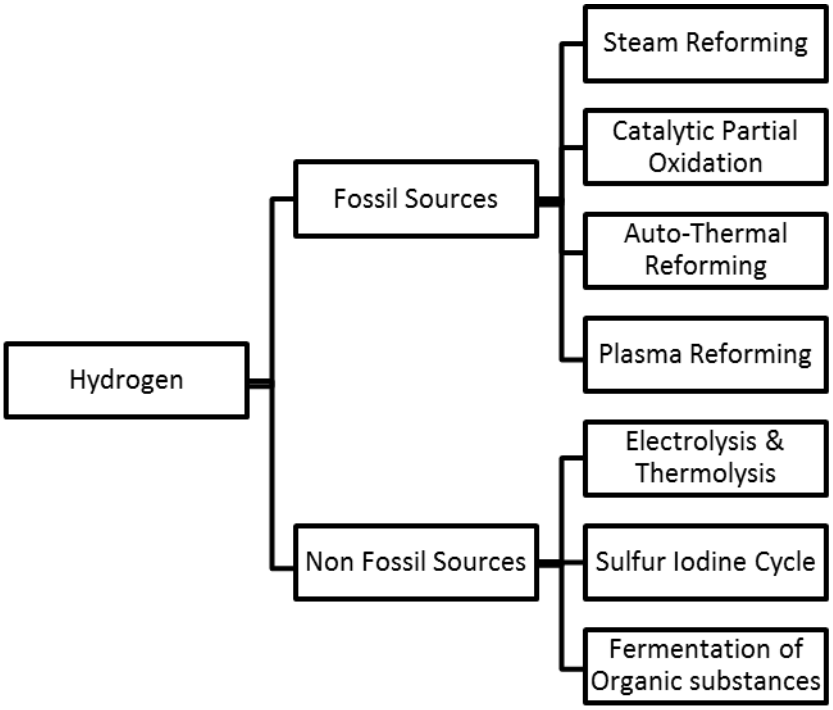

Figure 1.5 Hydrogen production technologies currently available

It is evident from Figure 1.5 that hydrogen can be produced from both fossil sources and non-fossil sources. And so, if we are able to find out a commercial method of producing hydrogen from non-fossil sources, we could pretty much solve the energy crisis. Since hydrocarbon infrastructure already exists and it is available economically at the moment, hydrogen production from hydrocarbons marks the starting point for the societal shift towards

hydrogen economy. However, it must be noted that hydrogen production from fossil fuels is just *a transitory process* and further research is required to produce hydrogen from carbon neutral sources.

The conversion of hydrocarbon fuels to H_2 is typically carried out by processes such as steam reforming (SR)-water gas shift (WGS), partial oxidation (POX) and auto thermal reforming (ATR). SR is a highly endothermic process requiring copious amounts of heat input. This also imposes constraints on the materials for the construction of the reactors. SR is generally accompanied by WGS in order to reduce/remove the presence of carbon monoxide in the reformate mixture [10].

$$CH_4 + H_2O \leftrightarrow CO + 3H_2, \quad \Delta H = +206kJ/mol \tag{1}$$

POX reaction is carried out at very high temperatures using sub-stoichiometric amounts of oxygen in the feed along with the fuel. Catalytic POX involves use of catalyst to improve the reaction rates at lower temperatures. POX however, produces lesser yield of hydrogen per carbon in the fuel.

$$CH_4 + \frac{1}{2}O_2 \rightarrow CO + 2H_2, \quad \Delta H = -36kJ/mol \tag{2}$$

ATR can be considered to be a hybrid of POX and SR and is a stand-alone process carried out in a single reactor. Its equipment complexity is the least amongst the three processes.

$$C_nH_mO_p + x(O_2 + 3.76N_2) + (2n - 2x - p)H_2O = nCO_2 + (2n - 2x - p + m/2)H_2 + 3.76xN_2 \tag{3}$$

In the equation (3), x defines the oxygen to fuel molar ratio and at x=0, the equation reduces to the endothermic steam reforming reaction; at x=n-p/2, the equation is nothing but the combustion reaction [11]. Clearly (3) represents the combination of the CPO and the SR. With various values of n, m and p, different hydrocarbon fuels can be considered.

The strong endothermic nature of SR makes the forward reaction favorable at higher temperatures while at lower temperatures, the backward reactions tend to become dominant. However, at higher temperatures the WGS is not favored since it is weakly exothermic as described in (4).

$$CO + H_2O \leftrightarrow CO_2 + H_2, \quad \Delta H = -41 kJ / mol \tag{4}$$

The SR is heat transfer limited and therefore fast heat transfer is essential to achieve reasonable conversion rates. In fuel cell applications, high conversion rates are desired since hydrogen is the primary fuel. The amount of steam supplied per carbon atom of the fuel decides the conversion of the hydrocarbon. Though high steam to carbon ratio (STCR) would greatly increase the conversion, the modern hydrogen plants are designed for STCR between 2.0 and 3.5 because higher steam increases risk of soot formation by lowering temperatures. Also, lower STCR's reduce the mass flow through the plant which leads to reduction in size of the equipment [10]. Hence, appropriate heating mechanisms are needed. The heating energy is supplied by preheating the feed of steam and fuel and also from heat transfer through the reactor walls from external combustion as in a heat exchange reformer (HER).

HER integrates the heat duties keeping the reactor compact while complicating the resulting flow arrangements [12]. However, the heat transfer in such a unit will be very fast since the heat generation from combustion and the heat removal from steam reforming occur directly at the thin catalyst coating on the metal surface. On a metal washcoat, heat transfer is through conduction which is much faster than standard convective heat transfer [13].

POX is exothermic and the use of fuel and air at high temperatures can favor the formation of coke which is harmful for the catalyst in fuel cells. POX reactors require external cooling systems and accurate flow control to prevent thermal run-away. Recently, catalytic POX reactors have been studied and it is found to operate at lower temperatures than non-catalytic POX and reduce the risk of coke formation [14].

ATR process integrates the endothermicity of the SR and the exothermic nature of the POX to give rise to a self-sustaining fuel processor that allows for a faster response to changing loads and start-up demands. Other advantages of ATR include simplified reactor model, wider choice of materials of construction and lower fuel consumption during start-up. Due to all these advantages, ATR seems to be the most efficient method to produce hydrogen for use in a fuel cell.

The reaction process used for on-board reformers depend on operating characteristics of the application such as 1) varying power demand 2) rapid startup 3) frequent shutdowns and the type of fuel cell stack under consideration such as Solid Oxide Fuel Cell (SOFC) or Proton Exchange Membrane Fuel Cell (PEMFC). The DOE has established long range performance targets for fuel processing systems [15]. There are various parameters that decide the performance of fuel processing systems such as the operating temperature and pressure, the reactor configuration, the fuel used, the catalyst used and the stoichiometric ratios of the fuel, steam and/or oxygen (if any). In this thesis, fuel processing systems for fuel cell applications are considered.

1.3 Thesis Overview

The objective of this research work is to design a computational model for the study of transient and steady state performance of an auto thermal reformer for application in an SOFC system. A small scale tubular reformer with coated catalyst is considered as the reactor. Methane, a light hydrocarbon rich in hydrogen is used as the fuel of choice since it is the predominant compound in U.S. natural gas. Natural gas has a well-established infrastructure and is economically viable. The catalytic effects have been avoided since it is strongly dependent on the type of catalyst and may vary greatly.

In this study, the following topics are discussed: 1) The results of systematic preliminary transient and steady state analysis of the SR of methane by considering experimental set up

using reservoirs, mixing chamber and pre-heater; 2) The results of transient and steady state analysis of the ATR of methane using the model based on SR system presented.

The organization of this thesis is now presented. A literature review along with the basic chemical concepts associated with reforming/fuel processing is presented in Chapter 2. The modeling of an SR system and a section explaining the modeling methodology of ATR is presented in Chapter 3. Chapter 4 presents the results and discussion of the SR and ATR systems. Chapter 5 presents the conclusions and finally, Chapter 6 makes recommendations for future work.

CHAPTER 2

LITERATURE REVIEW

2.1 Introduction

A typical fuel processor is explained in Figure 2.1. Processed hydrocarbon fuel is utilized in a fuel reservoir. The fuel and steam reservoirs are maintained at appropriate temperatures using primary preheaters. Mass flow controllers maintain the steam to carbon ratio in the fuel-steam mixing chamber. The mixture is raised to the appropriate temperature required at the inlet of the primary reformer wherein processes such as SR, POX or ATR convert the fuel and steam to hydrogen, carbon dioxide and carbon monoxide.

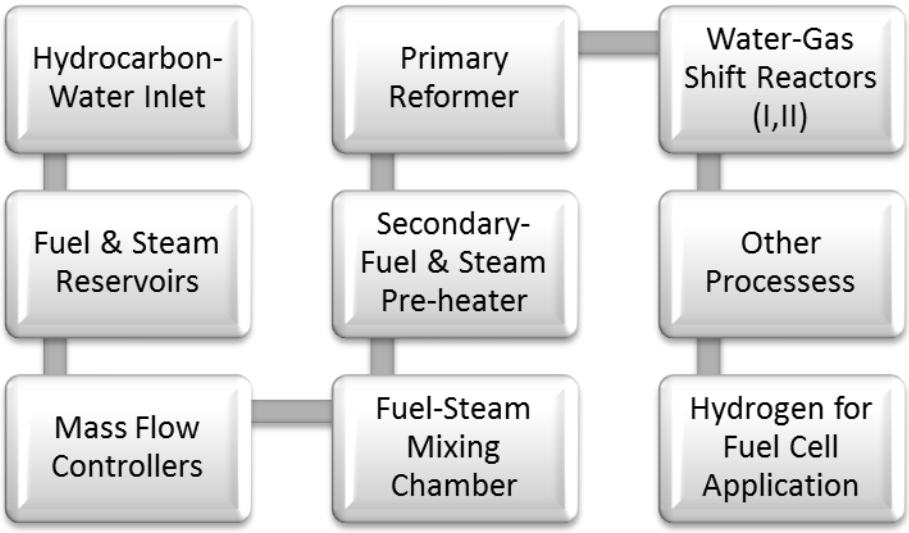

Figure 2.1 Schematic of a fuel processing system

The carbon monoxide in the reformate mixture exiting the primary reformer is further utilized by the low temperature shift (LTS) followed by high temperature shift (HTS) reactors. Other processes such as preferential oxidation or pressure swing adsorption can be used to

“clean” the reformate mixture in order to make the reformate mixture/hydrogen suitable for utilization in a fuel cell.

The block diagram shown in Figure 2.1 might appear simplistic. But implementation of the process is quite challenging, as at each block, the number of operating variables increase and those variables affect the overall system performance. For example, the fuel cell has to operate at varying loads and hence at different load conditions, different quantities of hydrogen must be supplied. To reciprocate to the load changes, the entire system must respond and this has to happen very quickly especially if the application is for on-board fuel processing. This necessitates investigation of the individual components that make up the system and their transient and steady state responses.

2.2 Previous Studies

The industrial steam reformers use large tubes loaded with fixed bed catalysts surrounded by external furnaces. There are a number of constraints on such reformers:

- Increased diffusional limitations with catalyst loading
- The thermodynamic limitations on the conversion of methane
- Carbon deposition and catalyst deactivation.

To overcome these limitations many improvements such as:

- Fixed bed with hydrogen perm-selective membranes
- Micro-channel steam reformer systems
- Bubbling fluidized bed reformer with/without hydrogen perm selective membranes [16]; have been suggested.

In the establishment of a distributed hydrogen infrastructure, hydrogen production on-site in small scale reactors is gaining attention as the reduction in size saves both cost and weight with the added benefit of having a smaller reactor to heat. It is well known that a metal monolith with catalyst coating on heat exchanger surface has good transient thermal response and can be operated either isothermally or with a gradient from inlet to exit. Also, the pressure drop across a coated metal monolith is significantly lower than that across a packed bed reactor making rapid reactions requiring shorter residence times more likely successful in the coated metal monolith [13].

Industrial SR is carried out in heated tubes/furnaces in the presence of nickel catalyst. Most of the noble metals (Ru, Rh, Pd, Ir and Pt) are also active but increase the capital. Reforming reactions are strongly affected by the catalyst. The number of moles of product per unit time depends on the active surface area of the catalyst. High surface area materials (100-400 m^2/g) are commonly employed in the preparation of catalysts. The chemical and physical properties of the catalyst influence its reactivity and stability. The method of preparation of the catalyst dictates its physical properties. The two most common methods of catalyst preparation include 1) impregnation of a metal salt in an aqueous solution onto a substrate/support and 2) co-precipitation of solution of metal salts added together at constant pH [17] . Catalysts are usually activated either by calcination or reduction.

Considering all these factors, just the chemical composition does not provide sufficient information regarding the effect of the catalyst. In fact, the number of molecules of product formed per unit surface area of a catalyst may vary by several orders of magnitude for essentially the same catalyst manufactured by different means.

Catalysts have to be reduced in an atmosphere of H_2 before reforming can be carried out. This is especially so in case of Ni catalyst since it is generally supplied in the form of NiO compound. Catalysts support the reactions only as long as there are active surfaces for the

reaction. These active surfaces may get blocked due to deposition of carbon or sulfur particles (poisoning) or due to sintering (thermal deactivation). If Ni is used as a catalyst, at high STCR oxidation causes the deactivation of the catalyst. Hence, activation and deactivation of catalysts play important role in the study of reformation.

Recently, the self-activation and self-regeneration property of certain precious metal doped Ni alloy was observed [18,19,20]. D. Li et al. [18], observed continuous regeneration of active Ni metal particles in Rh-doped Ni/Mg(Al)O catalyst due to reversible reduction-oxidation cycles. L. Zhou et al. [19] observed self-activation and self-regenerative activity performance in a Ru-doped Ni/Al2O3/alloy. Y. Zhan et al. [20] also verify the existence of such “intelligent properties” of catalysts by testing Pt/Ni/Mg(Al)O. These developments offer hope of finding catalysts that would work continuously without reduced activity even if subjected to daily start-up and shut-down procedures.

For ATR, the catalyst should retain its active surface at high temperatures and must be resistant to poisoning especially in the CPOX zone. The choice of the catalyst depends on the type of fuel used for the ATR. A large number of reforming catalysts have been developed at the Argonne National Laboratory (ANL) for the purpose of ATR for different hydrocarbon fuels. Hence, a wide variety of catalysts exist that can be used while designing a reactor.

The kinetics of chemical reactions is closely linked to the catalyst used. The values of parameters of the kinetic model and the fundamental reaction mechanism itself change with the composition of the catalyst, and this makes the development of a general kinetic model that can be applied to different catalysts impossible [21]. The reforming kinetics has been extensively studied over Ni catalysts. The various studies fall into three categories, namely, first order reaction with respect to methane, general Langmuir-Hinshelwood (LH) kinetics and Power Law expressions obtained by curve fitting.

Earliest works on the kinetics of SR of methane by Bodrov et al. [22] assumed that methane adsorption was the rate determining step. Later, Khomenko et al. [23] used the quasi-steady state approximation in terms of Temkin identity. Xu and Froment [24] conducted a series of experiments and came up with a complex Langmuir-Hinshelwood expression postulating that the reaction of adsorbed carbon and oxygen species is the rate determining step. However, it is now accepted that the dissociative adsorption of methane is the rate determining step [25]. Based on the mechanism predicted, the reaction parameters such as the activation energy and pre-exponential factor are determined. These reaction parameters are a combination of rate and equilibrium constants for several different elementary reactions.

The LH kinetics and the first order kinetics rely on simplifications and assumptions such as single rate determining step, one dominating species on the surface, quasi-equilibrium etc. To have an accurate picture, however, kinetic measurements of reforming reaction are normally fitted to the power law expression. The power law kinetics is often system specific and will not hold for other systems [26].

A much broader look at SR reveals that it has been extensively studied. J. Yuan et al. [27] present a three dimensional calculation method to simulate and analyze steam reforming of methane using a compact heat exchange reformer and the effects of various transport processes on reforming. Their model offers the possibility of determining the temperature and gas species distribution profiles by considering SR, WGS and Reverse Methanation. However, the paper assumes that the mole fraction of each reactant is known at the inlet.

A.K. Sunol et al. [12] investigated dynamic performance of a Heat Exchange Reformer (HER) suitable to be used with Proton Exchange Membrane fuel cell (PEMFC). Their paper focuses on dynamic response of HER for step variations in various input variables. The paper considers step changes in inlet gas flow rate, pressure and steam to carbon ratio without describing how the step changes can be effected in an experimental set up.

Abashar [28] discusses the coupling of steam and CO_2 reforming for production of hydrogen in the presence of two well-mixed catalysts in Fluidized Bed Reactor (FBR) and Fluidized Bed Membrane Reactor (FBMR). The optimal condition under which complete conversion of methane (99.8%) takes place decides the effective reformer length and this is used to evaluate the performance of the reactors. R. Hughes et al. [21] suggest that the increase in STCR favors forward reaction to produce CO_2 and inhibits the reverse water gas shift reaction that consumes CO_2. Thus, based on suitable operating conditions, a reactor model can be developed in which reverse water gas shift reaction is negligible.

In the various experimental studies [21] [29] , volumetric flow rate is used as independent variable controlling the reactor operating conditions or STCR. However, it is noteworthy that flow rate through the reformer cannot be controlled directly from fundamental law of gas flow physics, and the flow rate is a derivative property determined from reservoir pressures of the fuel gases and steam, and flow resistance of the downstream flow channels which can be controlled by opening or closing the valves. In that regard, direct control of STCR in the mixing chamber is also quite challenging due to unknown flow resistances of the reactor and upstream flow channels that connect the mixing chamber and fuel/steam sources, especially during transient operating conditions. During transient operating condition, flow resistance within the reformer also changes due to viscous change of the reacting flows.

In literature [30] [28], STCR is defined using flow rates of the each gas species into the mixing chamber instead of actual concentrations of these gas species in the mixing chamber and at reaction sites inside the reformer. Because of complicated reactions inside the reactor, site-specific local STCR within the reformer always deviates from optimal STCR and that from the mixing chamber.

Most of the authors in simulation studies [12,16,31] assume arbitrary STCR at inlet without considering actual hardware configuration of the reformer and flow control mechanism.

Therefore, it is not easy to verify their simulation models against typical experimental set up consisting of reactor, mixing chamber, and fuel gas/steam sources. .

In typical experimental procedure of reformer characterization involving certain desired STCR, fuel and steam pressures are controlled with fixed flow resistances (flow valves) to the mixing chamber or the flow resistances to the mixing chamber are adjusted with fixed fuel and steam pressures. In either approach, STCR in the mixing chamber is indirectly controlled. Implementation of active mass flow control devices along the fuel and steam lines is another way of controlling the mixing chamber conditions. However, from reformer designer's point of view, implementation of active mass flow control (MFC) devices to the mass-produced reformers is not economical. Therefore, computational model to address the design challenge of the reformer should be able to predict STCR in the mixing chamber accurately and also predict local temperature, pressure, and species concentration along the reactor flow channels properly.

In addition, the users of the computational tool may want to find right combination of the fuel/steam reservoir pressures and flow resistances (valve opening) to the mixing chamber from the fuel/steam reservoirs for certain user-specified STCR at the mixing chamber. Finally, it would be preferred to have the reformate gas at chemical equilibrium when it leaves the reformer. It depends on flow residence time (a function of flow speed) inside the reformer, which is a function of mixing chamber pressure, reformer geometry, and temperature inside the reformer flow channels. Therefore, more appropriate and physically reasonable computational model would require system level investigation considering transient dynamics of mixing chamber as well as the reformer itself.

This study was motivated by the needs of a realistic system level model to discuss the transient temperature and concentration profiles of the gas species and their distribution along

the reformer flow passage and the necessary pressures required in the fuel/steam reservoirs in order to satisfy the STCR conditions in the mixing chamber.

2.3 Challenges in Fuel Processing

Hydrogen is the lightest gas and has the smallest molecules compared to other gases; it can diffuse through many materials considered airtight or impermeable to other gases. This property makes the storage of hydrogen a challenging task [9]. It is a colorless, odorless and tasteless gas and leakages are very hard to detect. Besides, mercaptans used as smelling agents in LPG cannot be added to hydrogen for fuel cell use as they contain sulfur that would poison the catalysts in fuel cells.

Since the energy density of a fuel is a measure of how compactly hydrogen atoms are packed in a fuel, hydrogen gas has the least volumetric energy density compared to the conventional hydrocarbons that have more hydrogen atoms per molecule. Thus, for a given power, the volume of container required to store hydrogen gas is many times bigger than that required for storing a hydrocarbon fuel [9].

Considering this difficulty in storage, research efforts are underway in the area of on-board fuel processing technology for the production of hydrogen on-site by reforming of hydrocarbons.

There are several challenges in the fuel processing research such as reduction in cost of the fuel processing systems, prevention of catalyst deactivation, high yield of hydrogen and choice of fuel for a particular fuel cell. In several cases, it is highly desirable to remove the CO presence in reformate or sulfur in the feed which calls for improved technology. Cold-start and Fast-start are other problems that are being investigated.

CHAPTER 3

MATHEMATICAL MODEL

3.1 Introduction

The steam reformer system is modeled as a preheater-reformer assembly connected to a mixing chamber. The methane and steam reservoirs are connected to the mixing chambers indicated through mass flow controllers. Continuous heating is carried out to compensate for the endothermicity of the reaction. The steam reformer system is as shown Figure 3.1.

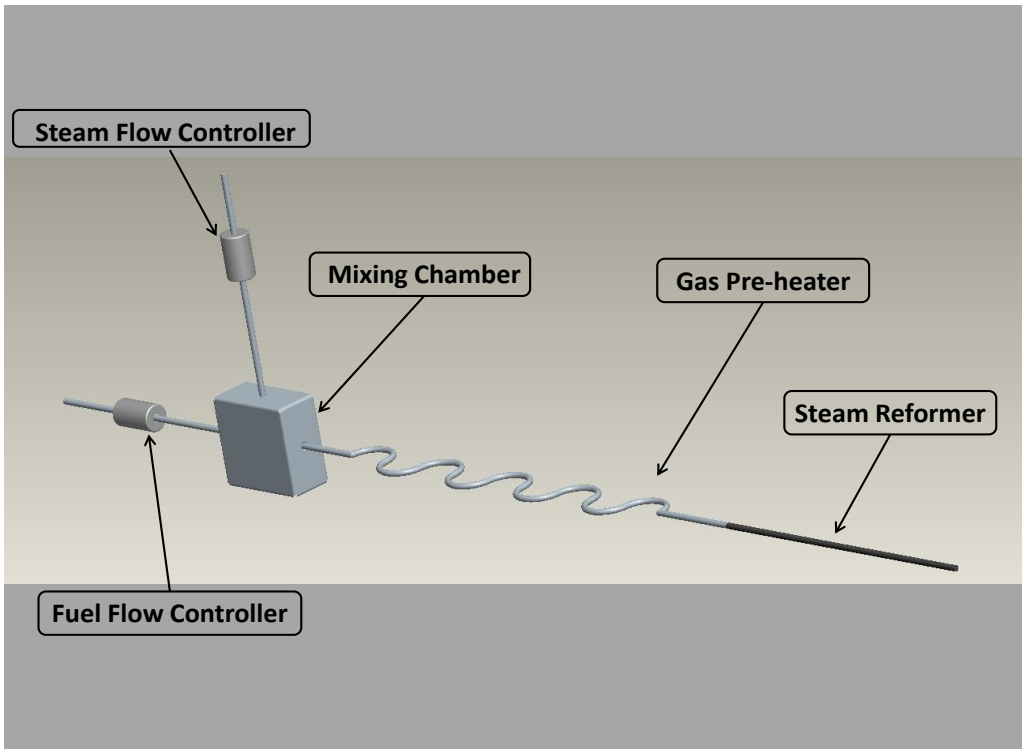

Figure 3.1 Physical model of the steam reformer system

The mixing chamber is modeled as an adiabatic chamber in which ideal mixing takes place. The preheater-reformer tube is modeled as a long tube with 1-D flow. The tube is divided

into 50 control volumes (CV) in all and the reformer section makes up 10 CVs while preheater makes up 40 CVs. The properties with-in each CV is assumed to be constant. An initial pressure gradient is fixed across the tube to initiate gas flow. Initial molar concentrations of each species inside the tube follow the air composition (21% oxygen and 79% nitrogen).

Initial gas flow is initiated by assuming certain linear pressure drop of ΔP across the reformer tube with respect to P_{exit} (atmospheric pressure in this study but can be assigned any arbitrary pressure depending on components attached to the downstream of the reformer). Then the reservoir pressure is selected to be a linear function of ΔP such that $P_{reservoir} = P_{exit} + \lambda_i \left(\Delta P\right)$. In addition to the initial pressure gradient, STCR ratio at the mixing chamber should be within certain range before fuel/steam mixture enters the first control volume of the reformer. By suitably tweaking λ_i (*i*=fuel and steam), appropriate STCR conditions in the mixing chamber can be created. For the simulation scheme, the STCR condition within the mixing chamber was limited between 2 and 3.5 by adjusting λ_i .

The mixing chamber pressure and downstream pressure at local control volumes within the reformer tube are found using mass continuity equations. During chemical reactions inside the reformer, localized pressure fluctuations are encountered and the pressures increase with temperatures. Since local reformer temperature changes, suitable pressure adjustment has to be made in the steam/fuel reservoirs in order to account for the change of back pressure in the mixing chamber, and also to maintain positive flow and desired STCR.

The modeling methodology is described in Figure 3.2. The initial conditions in the system such as temperature and the pressure are defined. The mass flow rate of each reactant species is evaluated in terms of pressure difference between the reservoirs and the mixing chamber and the steam to carbon ratio is computed. The control then passes to the STCR check wherein, decision is made so as to increase either fuel reservoir pressure, steam

reservoir pressure or if the STCR is appropriate the control passes back to mixing chamber and the properties are further evaluated in preheater and reformer sections.

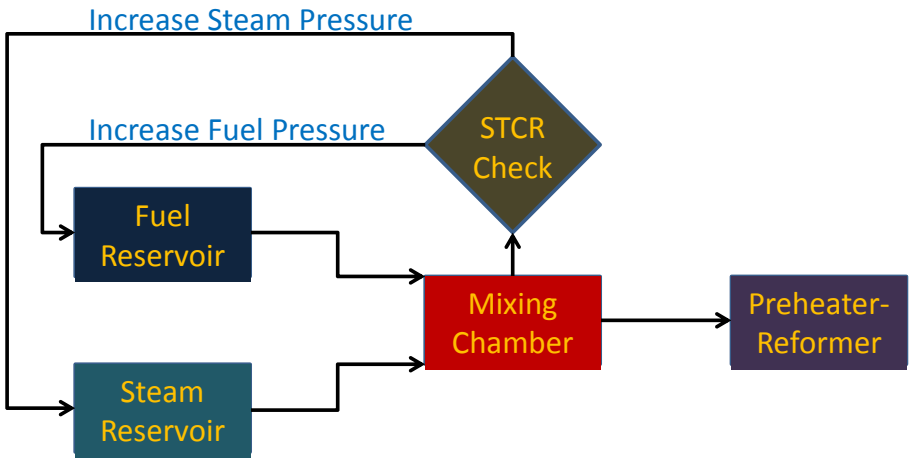

Figure 3.2 Schematic of modeling methodology

There are 3 state variables that are evaluated in a time marching scheme employing 4th order Runge-Kutta method. The temperature of the gas species, the temperature of the reformer/preheater walls and the molar concentration of each species described in terms of molarity forms the state variables.

3.2 Chemical Kinetics

The rate of a chemical reaction describes the quickness with which the reactants are consumed and the products are formed. The chemical kinetics is the study of rates of chemical reactions, the factors affecting them and their mechanisms [32]. The reaction rate is expressed in terms of disappearance of the reactants or the appearance of the products.

For a chemical reaction of the form

$$A + B \rightarrow C + D \tag{5}$$

the rate of the reaction is given by

$$Rate = k\left[A\right]^{x}\left[B\right]^{y} \tag{6}$$

Wherein, “x” and “y” are experimentally determined and “k” is the rate constant given by the “Arrhenius Equation” of the form

$$k_{\mathrm{j}} = A_{\mathrm{j}} \exp\left({-E_{a,\mathrm{j}}} \Big/ {RT_{wall,j}} \right) \tag{7}$$

“ A_j ” is the pre-exponential factor in mol/s, “ E_a ” is the activation energy in kJ/kmol, R is universal gas constant in kJ/kmol-K and T is the temperature in K. The activation energies and the pre-exponential factors of various chemical reactions are presented in Table 3.1.

Table 3.1 Summary of kinetic parameters [24]

Properties	Activation energy (kJ/mol)	Pre-exponential factor (mol/s)
Reforming reaction	240.010	$(4.225/3600)*10^{15}$
Shifting reaction	67.13	$(1.955/3600)*10^{7}$
Combustion reaction	-	10000.0

Often, chemical reactions occur simultaneously in opposing directions at the same rate and this state is known as chemical equilibrium. The equilibrium constant is a quantitative measure of the equilibrium which is constant at a given temperature and does not depend on the initial concentrations of the reactants or the products. It is generally presented in the form of “Van’t Hoff” equation which is suitably modified in terms of Gibbs potential as

$$K_p^j = \exp\left(\frac{-\Delta G_{rxn,j}}{RT_{\mathrm{wall,j}}} \right) \tag{8}$$

$\Delta G_{rxn,j}$ represents the Gibbs free energy change accompanying the reaction and is a function of enthalpy and entropy change accompanying a reaction at a given temperature.

$$\Delta G_{rxn,j} = \Delta H_{rxn,j} - T_{wall,j}\Delta S_{rxn,j} \tag{9}$$

The change in enthalpy and the entropy are given by the equations(10) and (11)

$$\Delta H_{\text{rxn,j}} = \sum \Delta H_{\text{products,j}} - \sum \Delta H_{\text{reactants,j}} \tag{10}$$

$$\Delta S_{\text{rxn,j}} = \sum \Delta S_{\text{products,j}} - \sum \Delta S_{\text{reactants,j}} \tag{11}$$

The enthalpy and entropy are calculated as shown in (12) and (13)

$$h_{f(T),i,j} = h_{f(298),i} + \int_{298}^{T_j} \hat{c}_{p,i}(T_j)dT \tag{12}$$

$$s_{(T),i,j} = s_{f(298),i} + \int_{298}^{T_j} \frac{\hat{c}_{p,i,j}}{T_j} dT - R_{univ} \int_{p(298)}^{p(T_j)} \frac{dP}{P_j} \tag{13}$$

Various ideal gas $\hat{c}_p$ values are calculated as function of absolute temperature using correlation (14)

$$\hat{c}_p = a + bT + cT^2 + dT^3 \tag{14}$$

Table 3.2 Correlation constants for computing specific heat of gases [41]

Species	a	b (*10^{-2})	c (*10^{-5})	d (*10^{-9})	Range (K)	Error (%)
CH_4	19.89	5.024	1.269	-11.01	273-1500	0.57
H_2O	32.24	0.1923	1.055	-3.595	273-1800	0.24
H_2	29.11	-0.1916	0.4003	-0.8704	273-1800	0.26
CO	28.16	0.1675	0.5372	-2.222	273-1800	0.37
CO_2	22.26	5.981	-3.501	7.469	273-1800	0.22
O_2	25.48	1.520	-0.7155	1.312	273-1800	0.28
N_2	28.90	-0.1571	0.8081	-2.873	273-1800	0.34

3.3 Heat Transfer Model

Heat transfer analysis is of utmost importance in any reformer system since it is the thermodynamics that controls the chemistry of the reactions. The thermal dynamics of the gas species consists of the enthalpy transported into and out of the control volume and the associated convection which is modeled as convective flow of the reactive gases (CFRG).

$$\frac{\partial T_{RF,j}}{\partial t} = \frac{1}{\sum_i [n]_{i,j}\, \hat{c}_{v,i,j}} \left\{ CFRG_j + \left(\sum_i [\dot{n}]_{i\_in,j}\, \hat{c}_{p,i,j} \right) T_{in,j} - \left(\sum_i [\dot{n}]_{i\_out,j}\, \hat{c}_{p,i,j} \right) T_{out,j} \right\} \tag{15}$$

Convective Flow of Reacting Gases (CFRG) is used instead of standard convection equation in the reaction zone. Convection can be visualized as the interaction of hot reacting gases at the wall surface producing cooler product gases with the exchange of thermal energy.

$$\begin{aligned} CFRG_j = & -\left[[\dot{n}]_{CH_4,j}\,|_{SR}\, \hat{c}_{p\_CH_4}(T_j) + [\dot{n}]_{CH_4,j}\,|_{SR}\, \hat{c}_{p\_H_2O}(T_j) \right] T_j \\ & -\left[[\dot{n}]_{CO,j}\,|_{WGS}\, \hat{c}_{p\_H_2O}(T_j) + [\dot{n}]_{CO,j}\,|_{WGS}\, \hat{c}_{p\_CO}(T_j) \right] T_j \\ & +\left[[\dot{n}]_{CH_4,j}\,|_{SR}\, \hat{c}_{p\_CO}(T_{wall,j}) + 3[\dot{n}]_{CH_4,j}\,|_{SR}\, \hat{c}_{p\_H_2}(T_{wall,j}) \right] T_{wall,j} \\ & +\left[[\dot{n}]_{CO,j}\,|_{WGS}\, \hat{c}_{p\_H_2}(T_{wall,j}) + [\dot{n}]_{CO,j}\,|_{WGS}\, \hat{c}_{p\_CO_2}(T_{wall,j}) \right] T_{wall,j} \end{aligned} \tag{16}$$

Reaction Enthalpy is the chemical energy released or absorbed during the reactions. This energy is added to the thermal equation of the wall since the reactions occur at the wall surface.

$$\begin{aligned} \dot{q}\,|_{SR+WGS,j} = & [\dot{n}]_{CH_4,j}\,|_{SR} \left(h_{f\_CH_4}(T_j) + h_{f\_H_2O}(T_j) - h_{f\_CO}(T_{wall,j}) - 3h_{f\_H_2}(T_{wall,j}) \right) \\ & +[\dot{n}]_{CO,j}\,|_{WGS} \left(h_{f\_CO}(T_j) + h_{f\_H_2O}(T_j) - h_{f\_CO_2}(T_{wall,j}) - h_{f\_H_2}(T_{wall,j}) \right) \end{aligned} \tag{17}$$

In the case of adiabatic mixing chamber, there is no thermal interaction with the walls and the transient equation is simply written as difference in enthalpies of the gas entering and gas leaving the mixing chamber.

$$\frac{\partial T_{chamber}}{\partial t} = \frac{1}{\sum_i [n]_i \hat{c}_{v,i}} \left\{ \left(\sum_i [\dot{n}]_{i\_in} \hat{c}_{p,i} \right) T_{in} - \left(\sum_i [\dot{n}]_{i\_out} \hat{c}_{p,i} \right) T_{out} \right\} \quad (18)$$

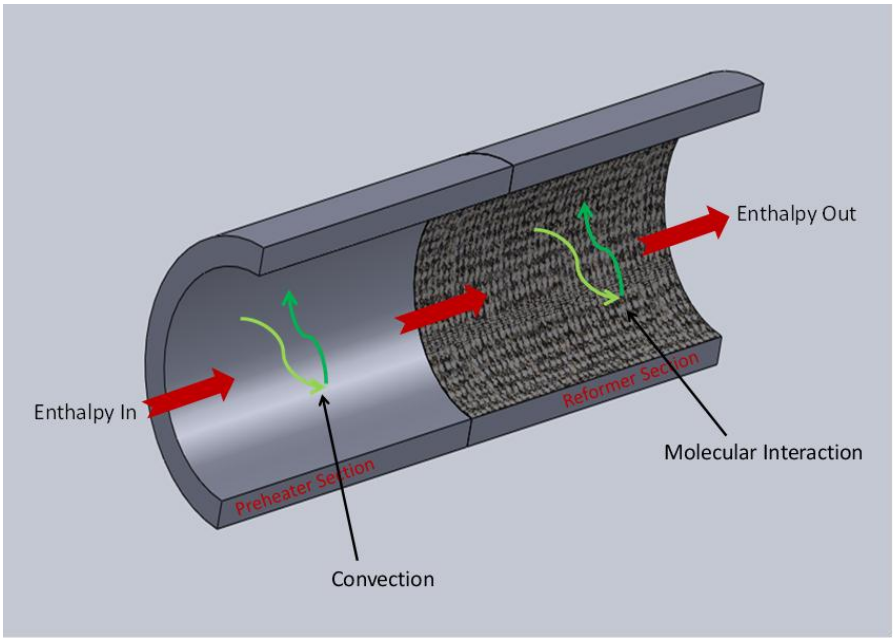

Figure 3.3 Heat transfer model for the gas flow

In the case of preheater, normal convection equation is considered instead of CFRG

$$\frac{\partial T_{preheater,j}}{\partial t} = \frac{1}{\sum_i [n]_{i,j} \hat{c}_{v,i,j}} \left\{ q_{convection,j} + \left(\sum_i [\dot{n}]_{i\_in,j} \hat{c}_{p,i,j} \right) T_{in,j} - \left(\sum_i [\dot{n}]_{i\_out,j} \hat{c}_{p,i,j} \right) T_{out,j} \right\} \quad (19)$$

$$q_{convection,j} = h_j A_{surface\_area,j} \left(T_{wall,j} - T_j \right) \quad (20)$$

In which $A_{surface\_area,j}$ is the inner surface area of the control volume of the reformer tube. Conduction is the fastest mode of heat transfer in a solid and hence it is indispensible.

The convection heat transfer for the reformer wall is written in terms of CFRG but with a negative sign in order to balance the net energy interaction between the wall and the gas.

Reaction enthalpy is added directly to the reformer wall and a constant heating term is introduced to counter the effects of strong endothermic reforming reaction. Constant heating is the net external heat supplied in order to maintain the temperature of the reformer wall. In most technical reviews, radiation is neglected since its effects are very hard to determine and strongly depend on the geometry and effective surface area of the system which vary greatly.

$$\partial T_{RF\_Wall,j} / \partial t = \left\{ \frac{k_{tube}}{\rho_{tube} \bar{c}_{v,tube}} \frac{\partial^2 T_{Wall,j}}{\partial x^2} \right\} + \frac{1}{\rho_{tube} \bar{c}_{v,tube}} \left[q_{heating,j} - \dot{q}_j \mid_{SR+WGS} - CFRG_j \right] \quad (21)$$

The walls of the preheater exchange thermal energy through conduction, convection and external heating as indicated in Figure 3.4. For the purposes of our study, the heating rate is assumed to be 1000 J/m^{2}s. A temperature control is applied in which the maximum temperature attainable by the preheater is limited to 800^{0}C or 1073 K.

$$\partial T_{preheater\_wall,j} / \partial t = \left\{ \frac{k_{tube}}{\rho_{tube} \bar{c}_{v,tube}} \frac{\partial^2 T_{wall,j}}{\partial x^2} \right\} + \frac{1}{\rho_{tube} \bar{c}_{v,tube}} \left[q_{heating,j} - q_{convection,j} \right] \quad (22)$$

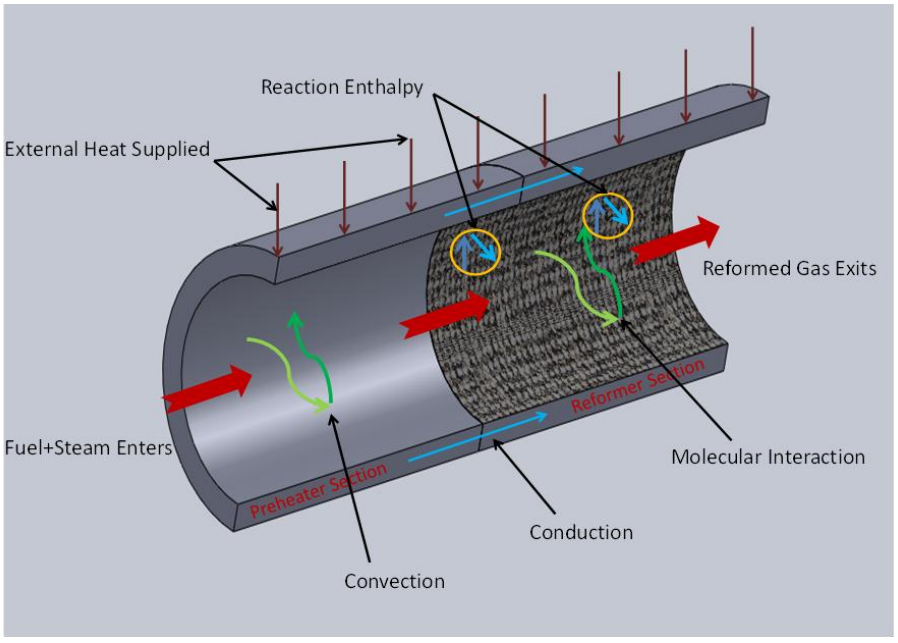

Figure 3.4 Heat transfer in solid structure

3.4 Transport Model

3.4.1 Dynamic Molar Balance Equations

Molarity Flux:

The physical transport of the gas species across various CVs is called the molarity flux. For every CV, there is a molarity flux entering and a molarity flux exiting the CV. The total molarity flux represents the molarity change in the bulk gas and is written in terms of mass flow rate which when multiplied by the mole fraction gives the gas species molarity flux:

$$\left[\dot{n}\right]_{i\_in\_j} = \frac{1000 y_{i,j} \dot{m}}{V_j \sum_i \left(y_{i,j} M_i\right)} \tag{23}$$

Conversion Rates:

When methane and steam are fed into a reformer, the conversion rate of methane into hydrogen by the reforming reaction is described using forward reaction rate as

$$\left[\dot{n}\right]_{CH_4,j}|_{SR} = k_{SR,j}\left[Q_{CH_4,,j} Q_{H_2O,j} - Q_{CO,j} Q^3{}_{H_2,j} \Big/ K_{p,j}^{SR}\right] \tag{24}$$

Similarly, the conversion rate of carbon monoxide into hydrogen by shift reaction can be described as

$$\left[\dot{n}\right]_{CO,j}|_{WGS} = k_{WGS,j}\left[Q_{CO,j} Q_{H_2O,j} - Q_{CO_2,j} Q_{H_2,j} \Big/ K_{p,j}^{WGS}\right] \tag{25}$$

The activities are functions of partial pressures given by

$$Q_{i,j} = \frac{y_{i,j} P_{total,j}}{P_{atm}} \tag{26}$$

Using the molarity fluxes and conversion rates described, a set of non-linear dynamic equations describing the molarity concentration in each CV can be written as indicated in (27).

General form:

$$\frac{\partial [n]_{i,j}}{\partial t} = [\dot{n}]_{i\_in,j} + \alpha_i [\dot{n}]_{CH_4,j}|_{SR} + \beta_i [\dot{n}]_{CO,j}|_{WGS} - [\dot{n}]_{i\_out,j} \quad (27)$$

The dynamics of molar concentration of each chemical species in each chamber of the reformer includes the inlet molar flow, exit molar flow out of the control volume and the molar conversion inside the control volume due to chemical reactions that follow molar stoichiometric coefficients α_i and β_i. The specific equations are:

$$\partial [n]_{H_2,j} / \partial t = [\dot{n}]_{H_2\_in,j} + 3[\dot{n}]_{CH_4,j}\Big|_{SR} + [\dot{n}]_{CO,j}\Big|_{WGS} - [\dot{n}]_{H_2\_out,j} \quad (28)$$

$$\partial [n]_{H_2O,j} / \partial t = [\dot{n}]_{H_2O\_in,j} - [\dot{n}]_{CH_4,j}\Big|_{SR} - [\dot{n}]_{CO,j}\Big|_{WGS} - [\dot{n}]_{H_2O\_out,j} \quad (29)$$

$$\partial [n]_{CH_4,j} / \partial t = [\dot{n}]_{CH_4\_in,j} - [\dot{n}]_{CH_4,j}|_{SR} - [\dot{n}]_{CH_4\_out,j} \quad (30)$$

$$\partial [n]_{CO_2,j} / \partial t = [\dot{n}]_{CO_2\_in,j} + [\dot{n}]_{CO_2,j}|_{WGS} - [\dot{n}]_{CO_2\_out,j} \quad (31)$$

$$\partial [n]_{CO,j} / \partial t = [\dot{n}]_{CO\_in,j} + [\dot{n}]_{CO,j}|_{SR} - [\dot{n}]_{CO,j}|_{WGS} - [\dot{n}]_{CO\_out,j} \quad (32)$$

Mixing Chamber and Preheater have no reactions and thus

$$\frac{\partial [n]_{i,chamber}}{\partial t} = [\dot{n}]_{i\_in,chamber} - [\dot{n}]_{i\_out,chamber} \quad (33)$$

$$\frac{\partial [n]_{i,preheater}}{\partial t} = [\dot{n}]_{i\_in,preheater} - [\dot{n}]_{i\_out,preheater} \quad (34)$$

3.4.2 Pressure Model

The computation of pressure at each instant is very critical in maintaining the required flow and also in the computation of "activities" of each species. The first step in the computation of pressure is the establishment of the initial mass balances. The "Mass Continuity Equation" is written in terms of the component pressures, average densities and average flow resistances.

$$\frac{\left(P_{CH_4}-P_{chamber}\right)\rho_{CH_4}}{R_{connecting\_tube1}}+\frac{\left(P_{H_2O}-P_{chamber}\right)\rho_{H_2O}}{R_{connecting\_tube2}}=\frac{\left(P_{chamber}-P_{exit}\right)\rho_{gas\_mix}}{R_{reformer\_tube}} \tag{35}$$

Equations (36), (37), (38) and (39) describe the computation of quantities used in (35).

The average density and viscosity of gas mixtures:

$$\rho_{gas\_mix}=\left(\sum_j \rho_j \Big/ Nz\right) \quad ;\mu_{gas\_mix}=\left(\sum_j \mu_j \Big/ Nz\right) \tag{36}$$

Density:

$$\rho=\frac{P}{R_{gas\_mix}T_{gas}} \tag{37}$$

Flow Resistance assuming laminar flow:

$$R_{reformer\_tube}=\frac{8\mu_{gas\_mix}L}{\pi r^4} \tag{38}$$

Chamber Pressure

$$P_{chamber}=\left(\frac{P_{CH_4}\rho_{CH_4}}{R_{connecting\_tube1}}+\frac{P_{H_2O}\rho_{H_2O}}{R_{connecting\_tube2}}+\frac{P_{exit}\rho_{gas\_mix}}{R_{reformer\_tube}}\right)\chi \tag{39}$$

$$\chi=1\Big/\left[\frac{\rho_{CH_4}}{R_{connecting\_tube1}}+\frac{\rho_{H_2O}}{R_{connecting\_tube2}}+\frac{\rho_{gas\_mix}}{R_{reformer\_tube}}\right] \tag{40}$$

Once the initial mass balances are established, the subsequent mass balance equation is used in the calculation of the actual pressure in the “Gauss Seidel subroutine”. The methodology is described in greater detail here.

Mass Balance

$$\frac{\left(P_{j-1}-P_j\right)\rho_{j-1}}{R_{j-1}}=\frac{\left(P_j-P_{j+1}\right)\rho_j}{R_j} \tag{41}$$

The simplification used in (42) allows for easier handling of the equations:

$$a_j=\frac{R_{j-1}\rho_j}{R_j\rho_{j-1}} \tag{42}$$

Actual Pressure

$$P_j=\frac{P_{j-1}}{1+a_j}+\frac{a_jP_{j+1}}{1+a_j} \tag{43}$$

Finally, by using the pressure terms computed so far, the actual value of chamber pressure is calculated by equations (44) and (45).

$$P_{chamber}=\left(\frac{P_{CH_4}\rho_{CH_4}}{R_{connecting\_tube1}}+\frac{P_{H_2O}\rho_{H_2O}}{R_{connecting\_tube2}}+\frac{P_1\rho_1}{R_1}\right)\phi \tag{44}$$

$$\phi=1\Bigg/\left[\frac{\rho_{CH_4}}{R_{connecting\_tube1}}+\frac{\rho_{H_2O}}{R_{connecting\_tube2}}+\frac{\rho_1}{R_1}\right] \tag{45}$$

3.4.3 Viscosity Model

A rigorous kinetic theory for monoatomic gases at low densities was developed independently by Chapman and Enskog. Their theory gives expressions for the transport

properties in terms of intermolecular potential energy. For non-polar molecules, the Lennard-Jones potential gives a satisfactory empirical expression, which is defined in terms of a characteristic diameter σ (known as collision diameter) and a characteristic energy ε. The parameter values are known for many substances and are presented in [33].

They can also be computed from the following equations:

$$\frac{\varepsilon}{\kappa} = 0.77 T_c \tag{46}$$

$$\sigma = 2.44 \left(\frac{T_c}{p_c} \right)^{1/3} \tag{47}$$

In which T_c is in Kelvin, σ is in Angstrom unit and p_c is in atmospheres.

Based on this, the viscosity of a pure mono-atomic gas of molecular weight M is given by:

$$\mu = 2.6693 * 10^{-5} \frac{\sqrt{MT}}{\sigma^2 \Omega_\mu} \tag{48}$$

Ω_μ which is a function of the dimensionless temperature $\frac{\kappa T}{\varepsilon}$ (or $\hat{T}$)and is interpreted as describing the deviation from rigid-sphere behavior of the molecules. The equation (48) is found to hold good for polyatomic gases as well. The parameter Ω_μ is calculated using the curve fitted model

$$\Omega_\mu = \frac{1.16145}{\hat{T}^{0.14874}} + \frac{0.52487}{\exp\left(0.77320 * \hat{T}\right)} + \frac{2.16178}{\exp\left(2.43787 * \hat{T}\right)} \tag{49}$$

The viscosity of a gas mixture is calculated using the semi-empirical formula

$$\mu_{\text{mix}} = \sum_{\alpha=1}^{\text{N}} \frac{x_\alpha \mu_\alpha}{\sum_\beta x_\beta \phi_{\alpha\beta}} \tag{50}$$

In which the dimensionless quantity $\phi_{\alpha\beta}$ is computed using

$$\phi_{\alpha\beta} = \frac{1}{\sqrt{8}}(1+\frac{\text{M}_\alpha}{\text{M}_\beta})^{-0.5} * [1+(\frac{\mu_\alpha}{\mu_\beta})^{0.5} * (\frac{\text{M}_\beta}{\text{M}_\alpha})^{0.25}]^2 \tag{51}$$

N is the number of chemical species present in the mixture and x_α is the mole fraction of species α. The formulae do not give reliable results for gases consisting of polar or highly elongated molecules because of the angle-dependent force fields that exist between such species. For polar vapors like H_2O an angle-dependent modification must be used. However, it is justifiable to use these relations as other considerations greatly increase the complexity of the computation.

3.5 Extension to ATR

Several studies on ATR indicate the current technology available. One of the most widely cited papers on ATR is from D. Papadias et al. [29]. They developed a transient multi-phase model for the ATR of gasoline. They also performed experiments in a micro-reactor system using rhodium deposited on gadolinium-stabilized ceria substrate as catalyst to validate the results of their start-up mode for partial oxidation, ATR using steam injection and ATR using liquid water spray. In the simulation they assume a mass-transfer limited combustion reaction i.e. $A_c \to \infty$. A similar approach is used in our combustion model by assuming a high pre-exponential factor value i.e. $A_c = 10,000.0$, in the combustion rate equation.

$$\left[\dot{n}\right]_j |_{CPOX} = A_{c,j} * y_{CH_4,j} * y_{O_2,j} \tag{52}$$

Hoang and Chan [34] investigated a Ni based catalytic reformer for ATR of methane. Their 2-D model tests the effects of Air/Fuel ratio and Steam/Fuel ratio on the performance and they present optimal values for the model.

J. Pasel et al. [35] have worked on the ATR of higher alkanes and Jet fuel. They designed three different types of reactors and analyzed the system performance with respect to the fuel used. ATR 5 was able to deliver a gas mixture of constant composition and quality when higher alkane was used as fuel. However, it was shown to be unsuitable for ATR of Jet A-1. Consequently, they developed ATR 7 and ATR 8 which were analyzed for optimal performance.

S. Roychoudhury et al. [36] designed and developed a diesel and JP-8 logistic fuel processor based on a modular catalytic Microlith ATR. The reactor under study demonstrated the capability of reforming liquid and gaseous hydrocarbon fuels at high power densities.

A. Mahecha-Botero et al. [37] tested a pilot scale FBMR under SMR and ATR conditions. They tested the reactor with and without perm-selective membranes and studied the reactor performance. They also investigated the effects of reactor pressure, hydrogen permeate pressure, feed flow rate and membrane load.

P.K Cheekatamarla et al. [11] analyzed ATR of synthetic diesel fuel in an adiabatic reactor using a Pt/ceria catalyst. They studied the product composition as a function of the operating variables and the temperature and concentration profiles inside the reactor. They also investigated the stability of the catalyst and its response to Sulfur poisoning.

M. Sommer et al. [38] modeled a fuel cell system and its components for locomotive application, using a 1-D ATR unit and considered gasoline reforming. They studied the dynamic response to load changes and suggested that its responses are too slow to be implemented in a

propulsion system. However, when integrated with a battery, a highly responsive ATR would reduce the cost of the battery in consideration.

M.H. Halabi et al. [39] presented a fixed bed reactor model and investigated ATR of methane. They predicted increased formation of hot spots for Oxygen/Fuel ratio greater than 0.5. However, they use a very high steam to carbon ratio of 4-6 which is not normally used in reformers.

As previously discussed, auto thermal reforming (ATR) can be visualized as a combination of steam reforming and partial oxidation reaction. However, there are many reactions that occur when a mixture of methane, air and steam is passed through a reactor. CO_2 reforming, methane cracking, and methanation are other reactions that occur along with steam reforming and partial oxidation. It has been reported [34] that some of these reactions have extremely slow kinetics compared to the others and hence are ignored. Total oxidation or combustion is a dominant reaction if there is a mechanism to light the mixture. However, it becomes dominating at elevated temperatures because of low auto ignition temperature (580 ^{0}C) of natural gas.

Hence, in the modeling of ATR, three dominant reactions have been considered. Total oxidation (combustion) followed by steam reforming and water-gas shift.

$$\begin{aligned} &CH_4 + 2O_2 \rightarrow CO_2 + 2H_2O, \\ &\Delta H_{298} = -890 kJ / mol \end{aligned} \tag{53}$$

The combustion reaction provides the heat required for the endothermic steam reforming. Hence preheater is not required in the case of the auto thermal reforming. The reactor design is relatively much simpler. The ATR is modeled as a mixing chamber connected to a reformer which is coated with reforming and shifting catalysts. The mixing chamber is connected to methane, steam and air reservoirs respectively through mass flow controllers that

control the respective flow rates depending on the steam to carbon ratio (STCR) and the oxygen to carbon ratio (OTCR).

The Heat Transfer Model for ATR is presented below:

$$\frac{\partial T_{chamber}}{\partial t} = \frac{1}{\sum_i [n]_i \hat{c}_{v,i}} \left\{ \left(\sum_i [\dot{n}]_{i\_in} \hat{c}_{p,i} \right) T_{in} - \left(\sum_i [\dot{n}]_{i\_out} \hat{c}_{p,i} \right) T_{out} - q_{combustion,j} \right\} \quad (54)$$

$$q_{combustion,j} = [\dot{n}]_j |_{CPOX} \left(h_{f\_CH_4}(T_j) + 2h_{f\_O_2}(T_j) - h_{f\_CO_2}(T_j) - 2h_{f\_H_2O}(T_j) \right) \quad (55)$$

It is the combustion enthalpy computed at the gas temperatures.

While in the reformer section,

$$\frac{\partial T_{RF,j}}{\partial t} = \frac{1}{\sum_i [n]_{i,j} \hat{c}_{v,i,j}} \left\{ \left(\sum_i [\dot{n}]_{i\_in,j} \hat{c}_{p,i,j} \right) T_{in,j} - \left(\sum_i [\dot{n}]_{i\_out,j} \hat{c}_{p,i,j} \right) T_{out,j} \right\} + \frac{1}{\sum_i [n]_{i,j} \hat{c}_{v,i,j}} \left\{ -q_{convection,j} - q_{combustion,j} \right\} \quad (56)$$

The convection is given by

$$q_{convection,j} = h_j A_{surface\_area,j} \left(T_j - T_{wall,j} \right) \quad (57)$$

While the heat transfer in the wall is given by:

$$\partial T_{RF\_Wall,j} / \partial t = \left\{ \frac{k_{tube}}{\rho_{tube} \overline{c}_{v,tube}} \frac{\partial^2 T_{Wall,j}}{\partial x^2} \right\} + \frac{1}{\rho_{tube} \overline{c}_{v,tube}} \left[q_{convection,j} - \dot{q}_j |_{SR+WGS} \right] \quad (58)$$

The molar balance equation is given by:

$$\frac{\partial [n]_{i,j}}{\partial t} = [\dot{n}]_{i\_in,j} + \alpha_i [\dot{n}]_{CH_4,j} |_{SR} + \beta_i [\dot{n}]_{CO,j} |_{WGS} + \gamma_i [\dot{n}]_j |_{CPOX} - [\dot{n}]_{i\_out,j} \quad (59)$$

γ_i is the molar stoichiometric coefficient for the combustion equation.

CHAPTER 4

RESULTS AND DISCUSSION

4.1 Preliminary Comparisons

The overall tube length considered was 1000mm and the tube was divided into preheater and reformer sections as previously explained in section 3.1. Results were analyzed for different tube lengths, at reformer inlet and initial temperatures of 400 ^{0}C and it was found that the computational model proved to be stable for values presented in Table 4.1 which are used for all the SR analysis.

Table 4.1 Steam reformer properties

Property	**Value**	**Unit**
Reformer length	200	Mm
Pre-heater length	800	Mm
Hydraulic diameter	4	Mm
Thickness	1	Mm
Tube density	8000	Kg/m^3
Specific heat	585	J/Kg-K
Thermal conductivity	22.8	W/m-K

As previously discussed in section 3.1, $P_{reservoir} = P_{exit} + \lambda_i \left(\Delta P\right)$ represents the reservoir pressure. The parameter λ_i was chosen to be 1.6 for methane and 2.3 for steam since with those values the initial STCR in the mixing chamber would be between 2 and 3.5.

Table 4.2 Initial fuel and steam reservoir pressures (gauge)

ΔP (Pa)	600	800	1000	1500	2000
Fuel Pressure(Pa)	960	1280	1600	2400	3200
Steam Pressure(Pa)	1380	1840	2300	3450	4600

Table 4.2 presents the initial pressures considered in the different pressure cases. In a given physical geometry, it is important to know the effects of various pressure gradients on the reforming capabilities. Also, in our computational model, the pressure directly controls the flow which decides the residence time. If the residence time of the gas is too low, there isn't enough time for thermodynamic and chemical interactions to take place, while, if the residence time is increased by a great extent, it leads to severe cooling which again affects the reforming ability of the device. In gas flows, the residence time is a very small value and small variations in their values cause considerable change in the reforming effects. The variations in residence times are imperceptible for our understanding and hence it is better to deal with pressure gradients that are much more perceptible.

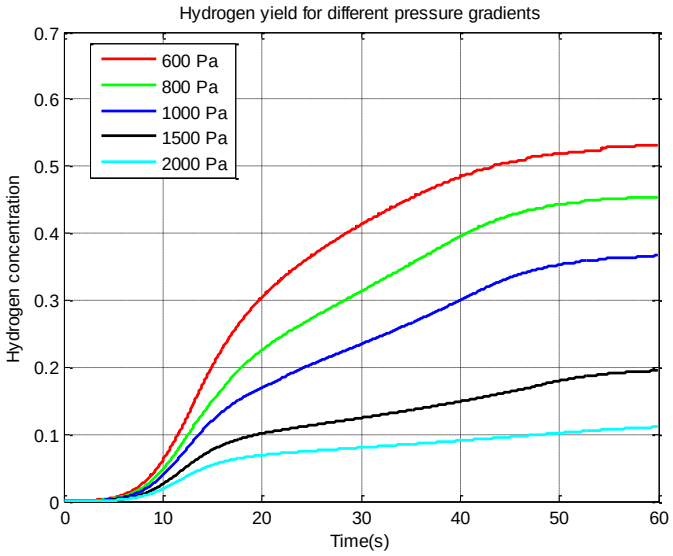

Figure 4.1 Hydrogen concentration as a function of time

The hydrogen yield as a function of ΔP is studied in Figure 4.1. From the figure, it appears that the case of 600 Pa produces the highest hydrogen. However, the overall mass or molar flow rate obtained decides the usefulness of the device rather than the mere percentage.

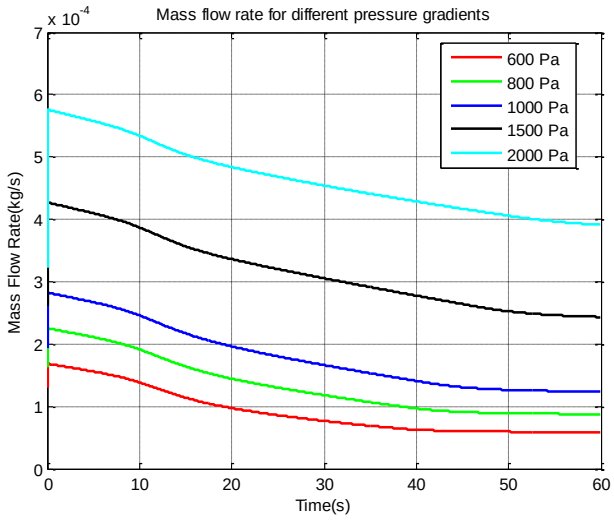

Figure 4.2 Mass flow rate versus time

Figure 4.2 represents the change in mass flow rate of all the gas species flowing through the preheater-reformer system.

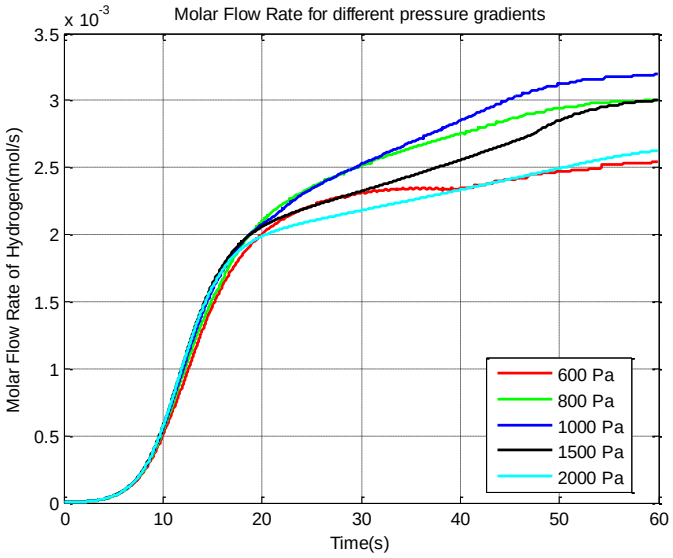

Figure 4.3 Molar flow rate versus time

Clearly the mass flow rate through the tube is directly proportional to the overall pressure gradient across the tube. It must be observed that for 600 Pa case, the mass flow rate is the least and hence, even highest concentration doesn't necessarily translate into highest molar flow rate of hydrogen. In Figure 4.3, molar flow rate reveals that the case of 1000 Pa gradient is the most beneficial in terms of hydrogen flow rate.

4.2 SR Evaluation

The 1000 Pa case is further evaluated to characterize the reformer. Thus, for the physical dimensions in consideration, we can assess the performance of the reactor. Simulations were performed keeping the 1000 Pa gradient and testing the reactor for different initial and inlet temperatures of (a) 400 ^{0}C (b) 600 ^{0}C.

(a) **(b)**

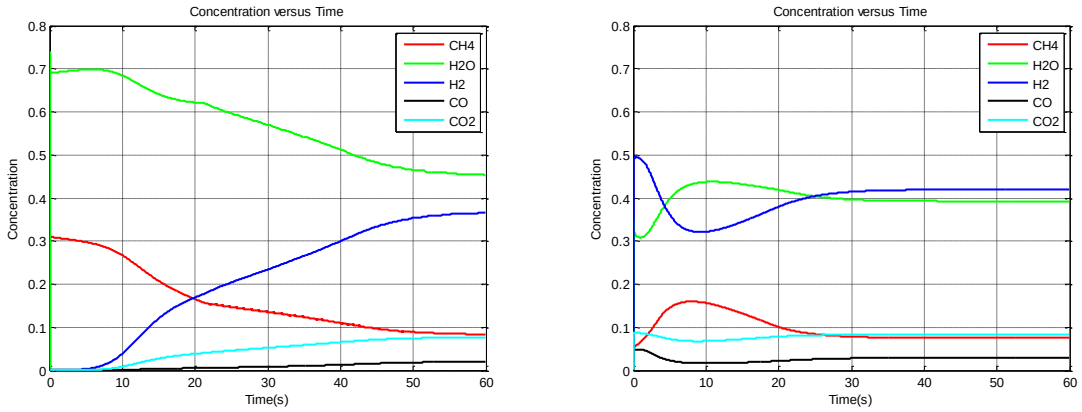

Figure 4.4 Species concentration at reformer exit (a) 400 ^{0}C (b) 600 ^{0}C

The concentration of different gases at the exit of reformer with respect to time is presented for the two cases in Figure 4.4. The mole fraction of the hydrogen is much higher in the case (b) indicating the strong effects of temperature on reformer. Also, it can be observed that the steady state of operation is reached in much shorter time for case (b).

The CO composition is around 3%, while the CO_2 composition is around 8%. From previous literature studies [10,13,24] it is known that the conversion of CO could be increased by decreasing the operating temperature. However, that requires implementation of an additional reactor to carry out the WGS which would make the fuel processor bulky. In case of a high temperature Solid Oxide Fuel Cell application, the CH_4 composition at the exit is reasonable.

The concentration of the gas species with length is presented in Figure 4.5. The plot was obtained by using the composition values at t = 60 seconds. The graphs look very similar except for the additional hydrogen obtained and steam consumed in case (b).

(a) **(b)**

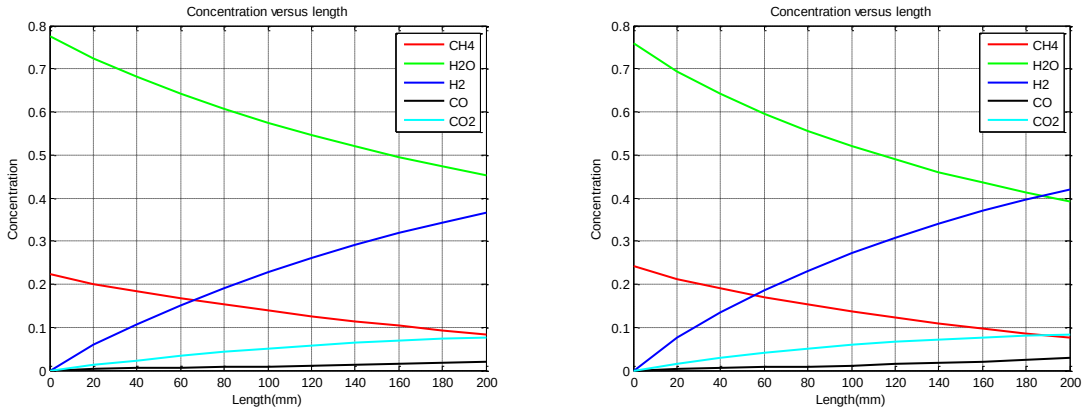

Figure 4.5 Gas species concentration along the reformer length (a) 400 ^{0}C (b) 600 ^{0}C

(a) **(b)**

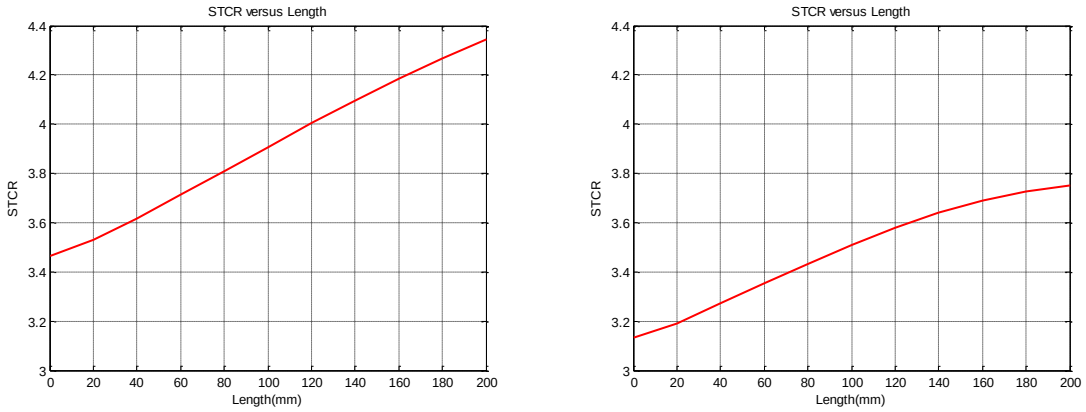

Figure 4.6 STCR along the length of the reformer at t=60s (a) 400 ^{0}C (b) 600 ^{0}C

The steam to carbon ratio inside the reformer is defined using steam and active carbon:

$$STCR = \frac{Steam}{Active\ Carbon} = \frac{y_{H_2O}}{y_{CH_4} + y_{CO}} \tag{60}$$

The steam to carbon ratio is an important parameter in reformer design. High STCR leads to cooling problems while low STCR leads to coking problems. If the variation of STCR is

large along the length of the tube, increasing the length of the tube turns out to be ineffective. As can be seen in Figure 4.6, the STCR along the length of the tube keeps increasing and in case (a), the STCR is much greater than 3.5. However, with increased temperature the gradient is much smaller. This implies that increasing the length of the reformer would require operation at much higher temperatures which adds to cost (especially catalyst) and heating problems.

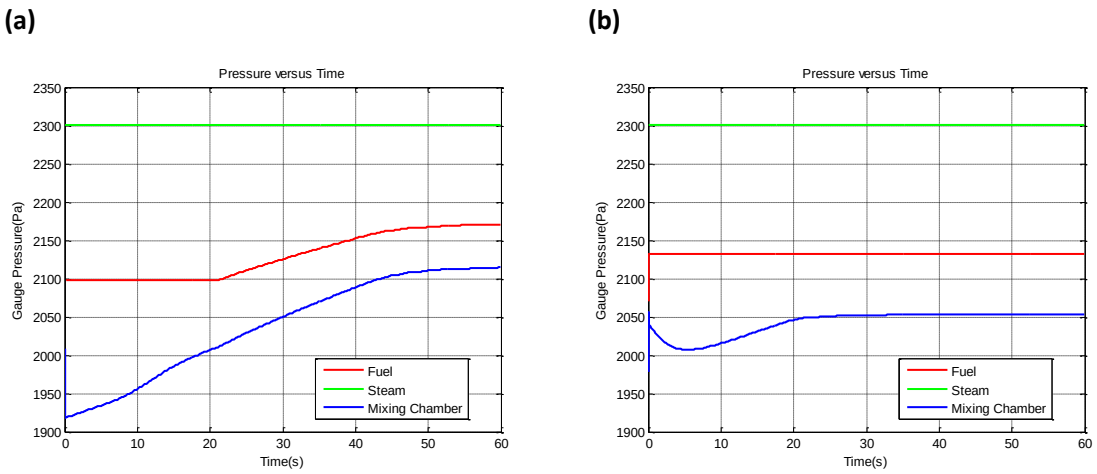

Figure 4.7 Reservoir pressures computed (a) 400 ^{0}C (b) 600 ^{0}C

It is important to investigate the success of the algorithm implemented to capture reservoir pressures required to maintain the STCR in the mixing chamber. From Figure 4.7 it is evident that the steady state gauge pressures are: Case (a):1) Fuel Reservoir - 2171 Pa 2) Steam Reservoir - 2301 Pa 3) Mixing Chamber - 2115 Pa; Case (b): 1) Fuel Reservoir - 2132 Pa 2) Steam Reservoir – 2301 Pa 3) Mixing Chamber - 2053 Pa. These pressures are controlled by STCR control as described in Figure 4.8.

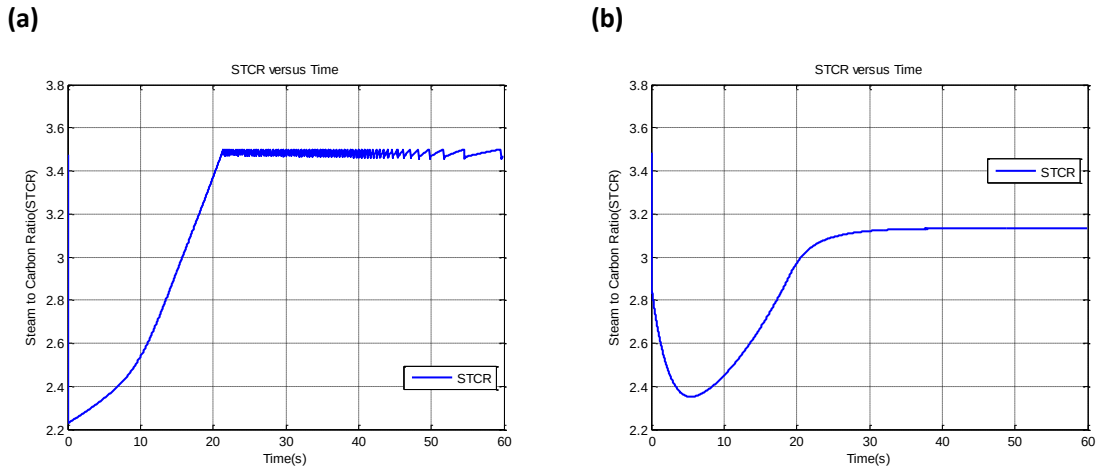

Figure 4.8 STCR in the mixing chamber (a) 400 ^{0}C (b) 600 ^{0}C

While the STCR operates at the upper limit at lower temperatures, as the temperature is increased, the STCR becomes steady at a much lower value. The pressures obtained within the preheater and reformer tube are derivative properties making use of the pressure predicted in the reservoirs by STCR control. The overall pressure distribution is presented for the two cases in Figure 4.9.

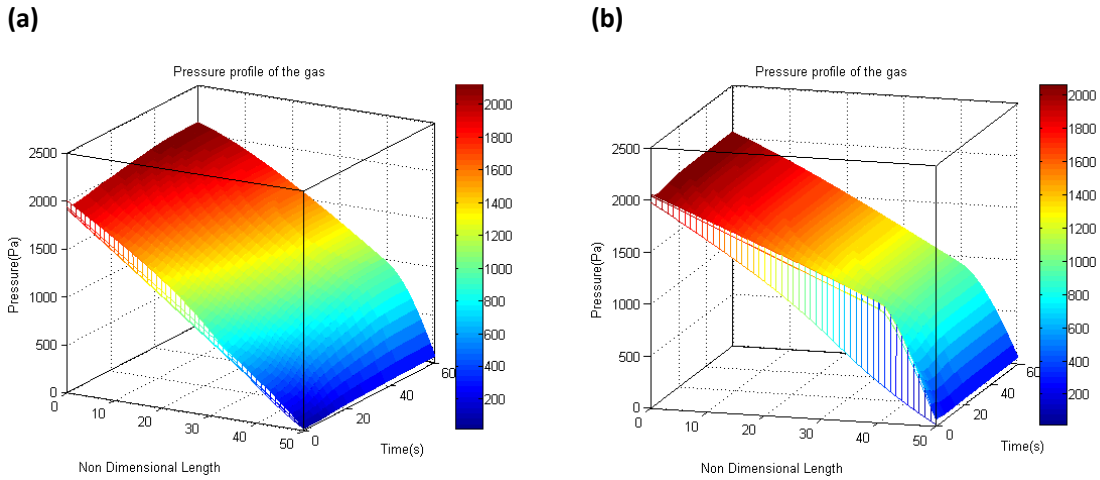

Figure 4.9 Pressure profile in preheater and reformer sections (a) 400 ^{0}C (b) 600 ^{0}C

The knowledge of temperature distribution in the tube is critical in order to predict/provide heat addition required to compensate for steam reforming. The gas temperature shows a steady increase along the preheater length and drops suddenly at the reformer section. The long preheater was used because the heat transfer obtained under laminar flow is lesser than the heat transfer under turbulent flow conditions. For turbulent flow, higher flow velocities have to be used that change the component requirements and are left out of consideration in our simulation model.

(a) **(b)**

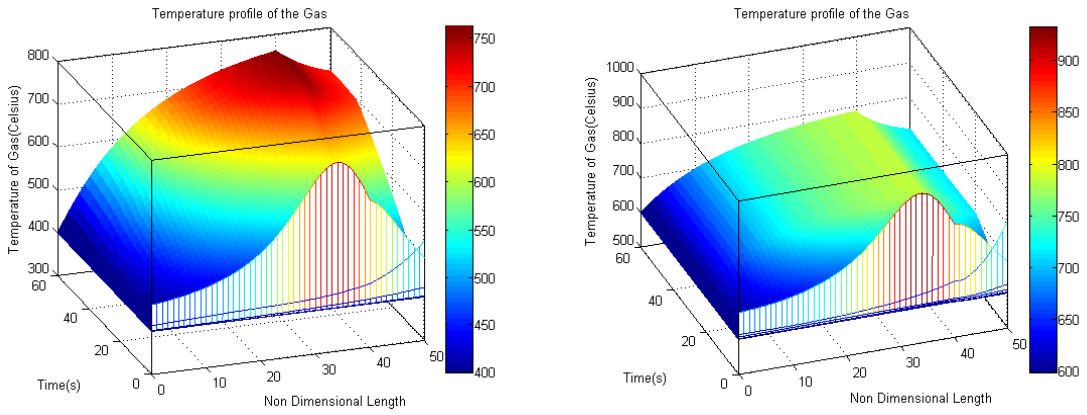

Figure 4.10 Temperature profile of the gas (unedited) (a) 400 ^{0}C (b) 600 ^{0}C

Since the tube is initially filled with oxygen, there is a high possibility of localized transient combustion that needs to be addressed in greater detail. The transient peak observed in the gas temperatures is ascribed to the complicated heat interactions of the incoming fuel and steam with the outgoing oxygen and nitrogen. During the computational analysis, it was found that the “specific heat” values were important parameters in the success of the transient analysis. The sudden changes in specific heat values due to impingement of new gases could be a cause for the initial peaks. However, the initial transient peak dies down within milliseconds (8 iterations) of operation and the gas temperature reaches the initial/inlet temperatures. This

indicates that the transient peak might not even be detected in reality if it is a part of physical process. Or, it may be due to the numerical computational scheme itself. In any case, the overall result of isn't affected by the initial transient peak. The edited gas temperature profile in which the first 8 iterations have been discarded is presented in Figure 4.11.

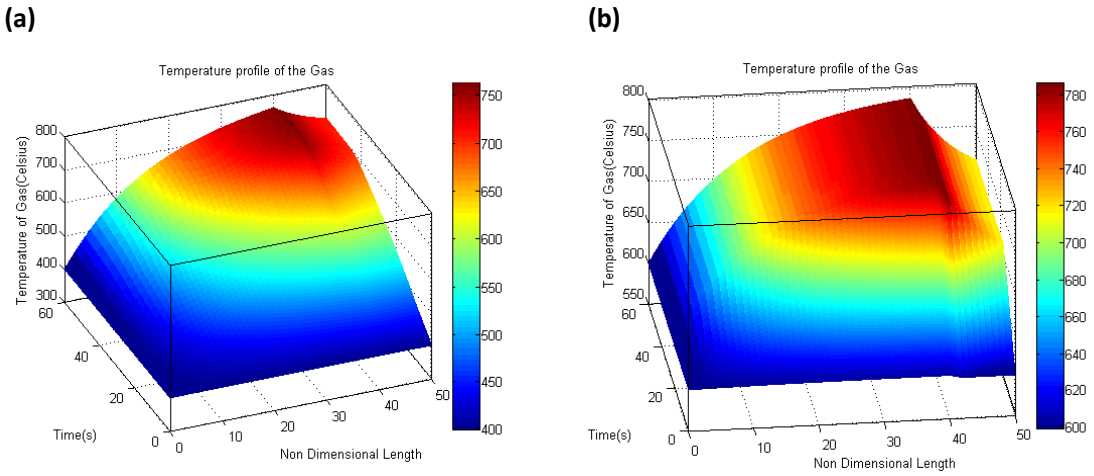

Figure 4.11 Temperature profile of the gas (edited) (a) 400 ^{0}C (b) 600 ^{0}C

The wall temperature distribution indicates the sudden drop in temperature obtained due to the highly endothermic nature of the steam reforming reaction occurring at the catalyst/wall of the reformer section. Since discretized model was used, the temperature drop appears to be that rapid, while in reality, the temperature gradient expected might be a little smoother. A temperature control was used to provide heating only up to 1073 K. The heating rate utilized was 1000 W/m^2.

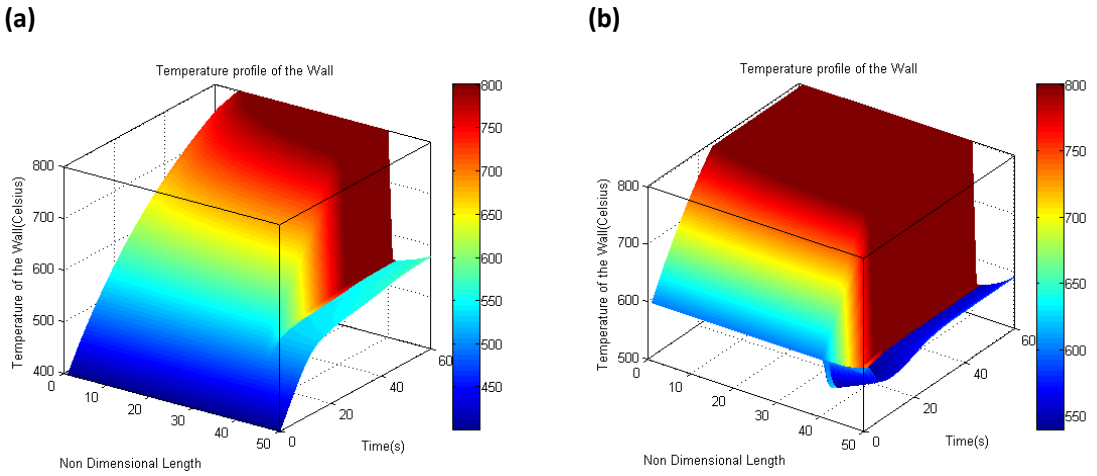

Figure 4.12 Wall temperature profile (a) 400 ^{0}C (b) 600 ^{0}C

The parameter CO/H_2 indicates the ability of the reformer to carry out WGS. It is seen that the steady state ratio obtained is much higher for case (b) which reflects the weakly exothermic nature of WGS. Smaller the CO/H_2, better is the WGS capability.

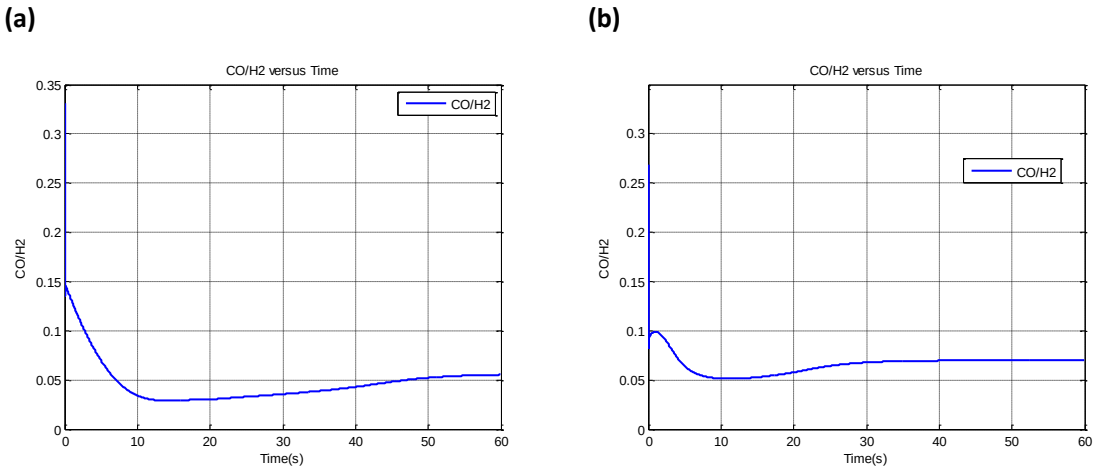

Figure 4.13 CO/H2 at the end of the reformer (a) 400 ^{0}C (b) 600 ^{0}C

In literature, there are several definitions for conversion of methane. The simplest one:

$$Conversion = \frac{\dot{n}_{CH_4\_in} - \dot{n}_{CH_4\_out}}{\dot{n}_{CH_4\_in}} \tag{61}$$

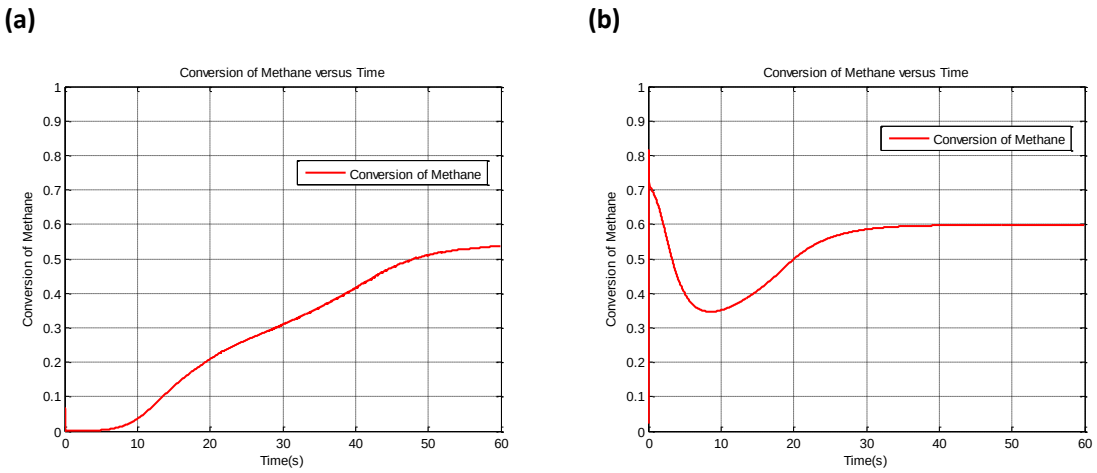

Figure 4.14 Conversion of methane obtained (a) 400 ^{0}C (b) 600 ^{0}C

From Figure 4.14, it can be seen that higher temperature leads to higher conversion. It is also evident that for the kinetic parameters under consideration, the reforming reaction rate is insignificant at temperatures around 400 ^{0}C while the reforming rate is significant enough around 600 ^{0}C since the reforming causes sudden drop in temperatures. The heat transfer model considered, thus, works well at higher temperatures when the reaction rates are higher as opposed to lower temperatures.

Finally, it is observed from Figure 4.15 that the overall molar flow rate of hydrogen isn't affected by temperature but the steady state is reached rapidly in case (b).

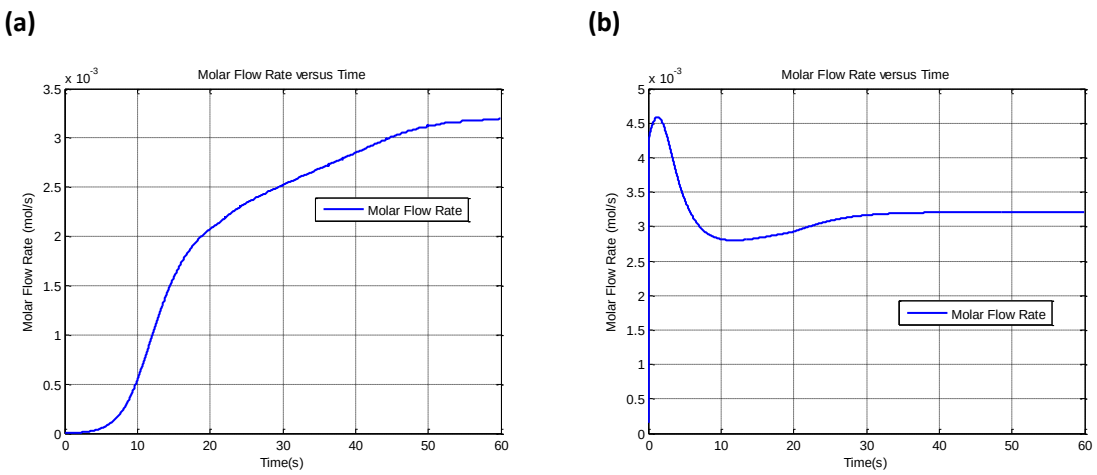

Figure 4.15 The molar flow rate of hydrogen with time (a) 400 ^{0}C (b) 600 ^{0}C

4.3 ATR Evaluation

The ATR reactor is exactly similar to that of the steam reforming reactor. Instead of considering a 1000mm tube with 200 mm reformer section, the ATR is modeled as a 300 mm reformer tube without preheater. All the other properties remain the same as given in Table 4.1

Typically air is passed in the reactor along with steam and fuel to cause combustion (partial/total). In our evaluation, total combustion is considered since at the temperatures considered (600 ^{0}C) the fuel-air mixture would automatically light-off and total combustion would be the dominant reaction. The hydrogen yield in ATR depends on the temperature of operation which in turn depends on the air flow rate in the inlet stream. The gas concentration is presented in Figure 4.16.

The benefit of ATR operation is that no external heating is necessary in steady state of operation. That however, comes with the cost that the hydrogen yield obtained is much lesser than the case of steam reforming. Also, ATR mode operation involves the additional burden of Air to Fuel Ratio or typically Oxygen to Carbon Ratio (OTCR) control. Too much of oxygen in the feed leads to consumption of the fuel by combustion leading to decreased reforming.

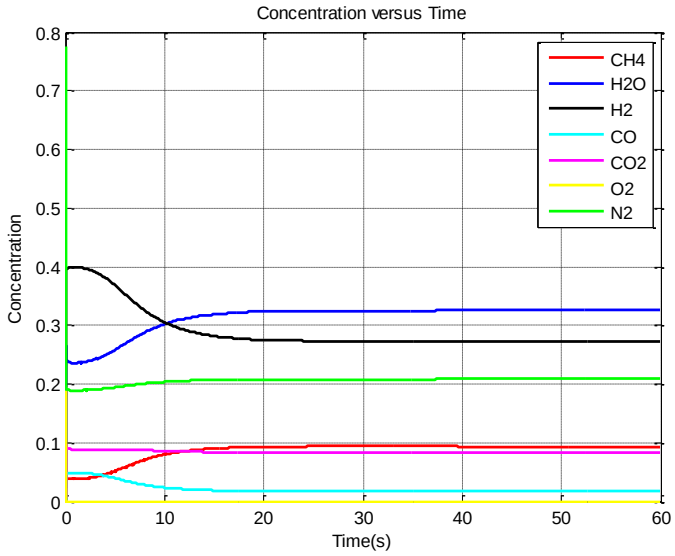

Figure 4.16 Species concentration in ATR mode

Similarly, if the reactor is operated in lean air mixtures, there is a chance that reactions in the reactor might stop owing to decreased temperatures due to reformation. Therefore, ideal OTCR is essential for maintaining the reactor under constant operation.

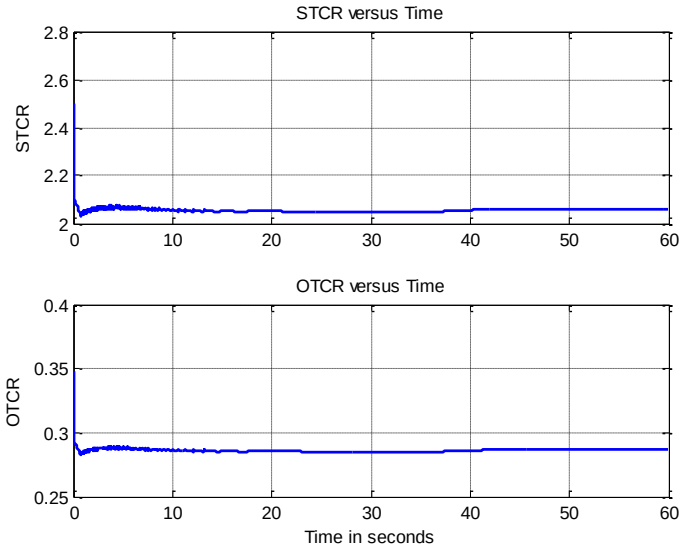

Figure 4.17 STCR and OTCR control obtained

In our simulation model, the STCR is controlling factor for reservoir pressures and consequently the overall mass flow rate (Figure 4.18).

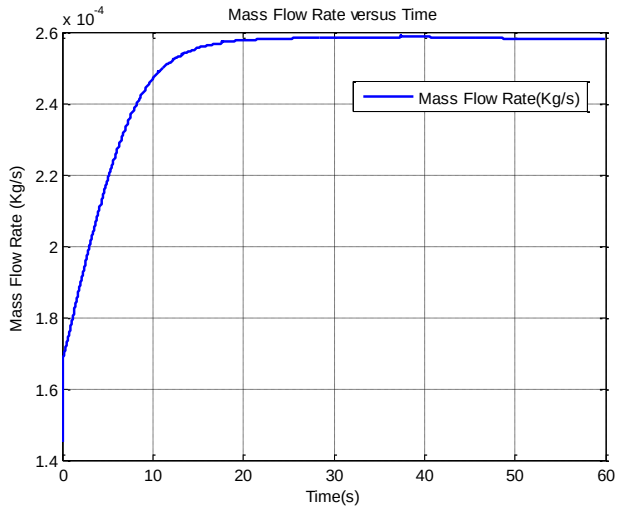

Figure 4.18 Mass flow rate as a function of time

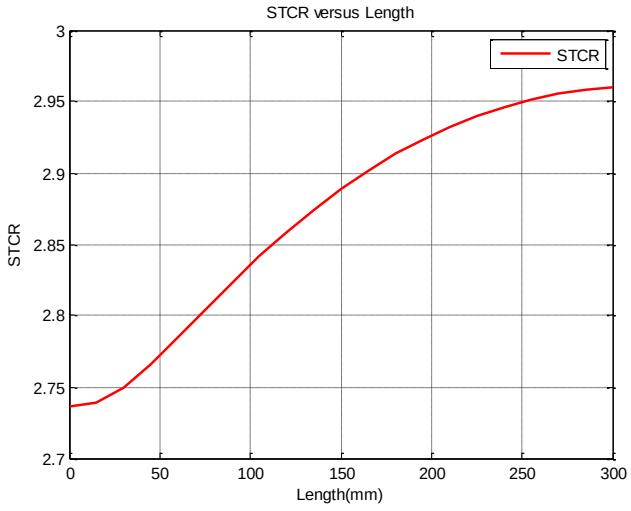

Figure 4.19 STCR versus length at t=60s

The STCR is maintained between 2 and 2.5 in mixing chamber. When the STCR goes below 2, the steam reservoir pressure and simultaneously the oxygen reservoir pressure is

increased. This range of control is highly efficient since the overall STCR along the length of the reformer doesn't change significantly as indicated in Figure 4.19.

The reservoir pressures that maintain STCR/OTCR and hence sustaining reactor:

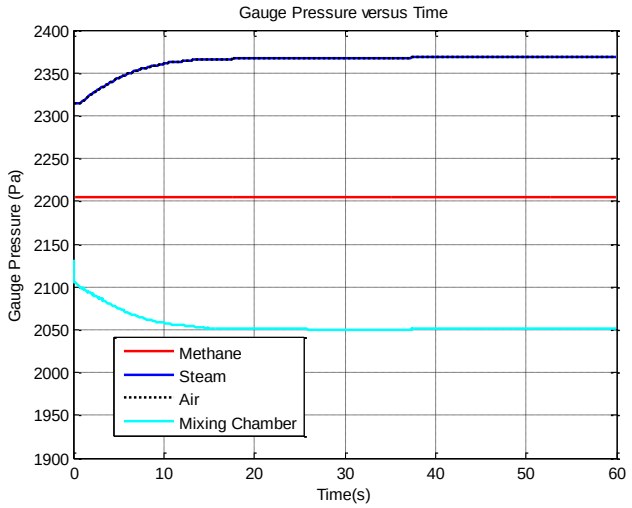

Figure 4.20 The reservoir pressures required to maintain STCR/OTCR

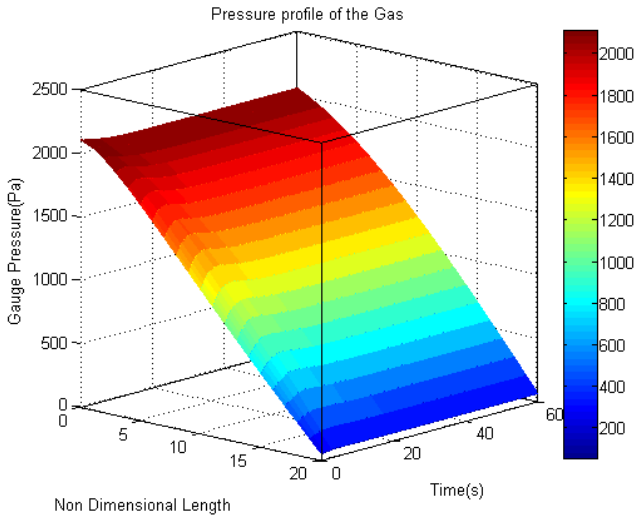

Figure 4.21 Gas pressure profile in the reformer

The pressure calculation algorithm is same as that used in steam reforming case. The Gauge pressure profile is presented in Figure 4.21. The pressure profile of the gas looks similar to the temperature profile indicated in Figure 4.22.

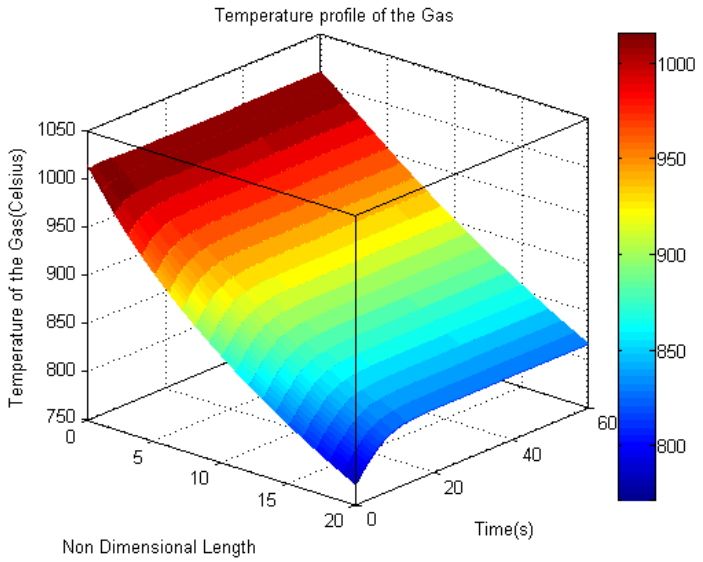

Figure 4.22 Temperature profile of the gas

It is important to note that the initial spike obtained is not presented since that does not change the veracity of the transient results. There is a significant drop in temperature along the length of the reactor. The large temperature drop reflects the thermal differences between combustion and reforming. Significant gradients in temperatures may cause thermal instability problems.

A novel approach was used by Huppmeier et al. [40] to solve the hot spot problems in the case of oxygen premixed with the feed gas stream. They presented the concept of oxygen injection at different locations through oxygen feed membranes. They developed a theoretical model that predicted almost 100 percent isothermal operation. Consequently, experimental analysis in small scale reactors resulted in just 5K deviation from isothermal behavior without

losses in the conversion rate or changes in hydrogen or carbon monoxide selectivities. They also present an ideal premix to obtain optimal results.

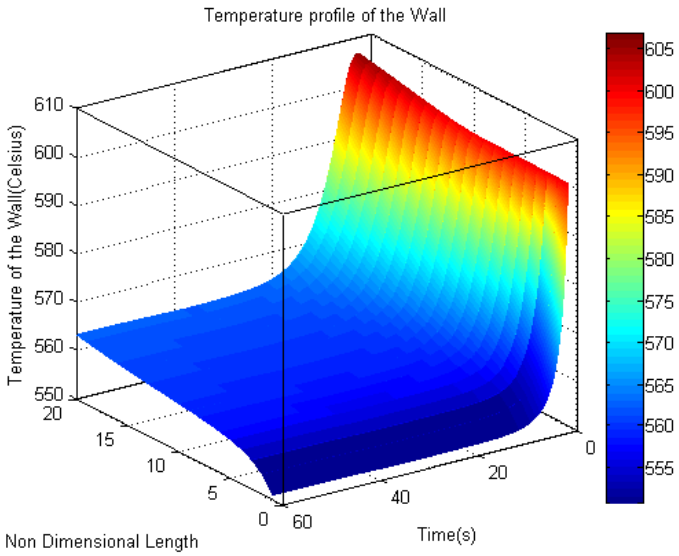

Figure 4.23 Temperature profile of the wall

The thermal gradients in the reformer wall Figure 4.23, are not so significant in our model since laminar flow model of the gas is used which reduces the overall heat transfer coefficient. The heat transfer coefficient would make a significant difference in the local wall temperatures and the corresponding reforming reaction rates. However, considering the small tube and the other operating conditions, modeling localized turbulent flow due to combustion would complicate the analysis.

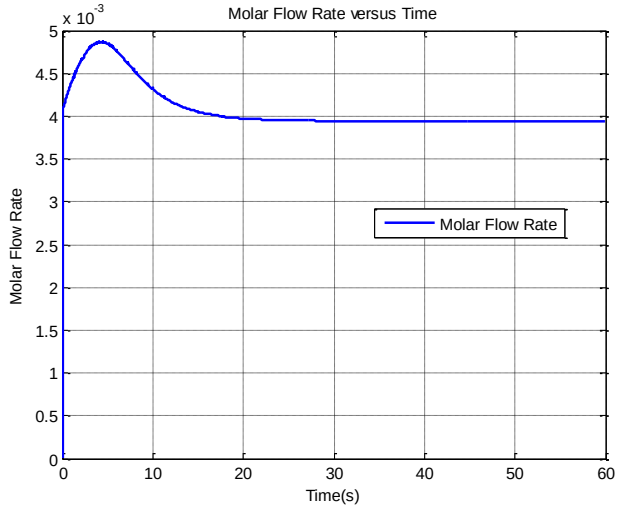

Figure 4.24 Molar flow rate of hydrogen

The molar flow rate of hydrogen with respect to time, Figure 4.24 and the ratio of carbon monoxide and hydrogen at reformer exit with respect to time, Figure 4.25 conclude the analysis of the reformer. Favorable molar flow rate and CO/H_2 values are predicted for the reformer in ATR operation.

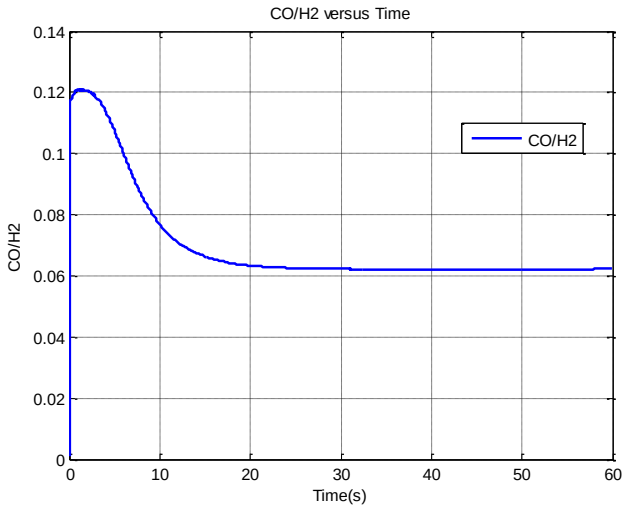

Figure 4.25 CO/H2 versus time

CHAPTER 5

CONCLUSIONS

The computational models presented in this study enable scientists and practicing engineers to optimize the design of steam and auto-thermal reformers.

A 1-D model of a steam reformer with built in preheater and connected to fuel and steam reservoirs through mixing chamber and connecting tubes has been designed. The physical system was evaluated for optimum pressure gradient to achieve maximum molar flow rate of hydrogen. Using the optimum pressure gradient, the system was then evaluated at two different temperatures and the various system characteristics were observed.

The computational model predicted the transient and steady state values of gas temperature and pressure, wall temperatures and the gas concentration in the mixing chamber, preheater and reformer. The model enabled prediction of the reservoir pressures required to maintain appropriate STCR in the mixing chamber. The STCR along the reformer was computed which emphasizes the usefulness of the tool in optimizing design.

The SR model was extended to consider ATR case. This reflects the flexibility of the computational model which can be easily manipulated to consider different forms of reactions and heating mechanisms. Combustion of methane provided the heat for reforming reaction. The ATR results for a specified temperature were reported in terms of gas species composition, pressure and temperature and the wall temperature along the length of the reformer. The pressures in the reservoirs required to maintain appropriate STCR and OTCR were computed to obtain a sustaining reactor.

The models present novel implementation of heat transfer laws for the modeling of reactive flows within reformers. Such an implementation can be applied to any system in which chemical reactions occur on the wall/catalyst surfaces.

CHAPTER 6

SCOPE FOR FUTURE WORK

It is the responsibility of scientists and engineers to create efficient energy conversion devices for sustainable and environmentally friendly development. While the computational model presented in this document serves as an effective tool to manipulate physical structures/input conditions to obtain optimum design, there are additional enhancements that could increase the performance of this tool.

In the literature review, we have reported that the catalytic properties play a very significant role in deciding the kinetics of the reactions. Inclusion of catalytic effects through characterization of the coating and reaction mechanisms could improve the model drastically. The coating effect on the flow resistance is ignored and laminar flow is considered in the simulation. By characterizing the coating, a better picture of the kinetic model could be obtained. Radiation has been avoided in the thermal model owing to its complexity. In high temperature systems, radiation heat transfer plays a significant role. Considering the radiation effects could improve the result. Also, the heat transfer coefficient could be found out as a function of local Reynolds number. Specifically, in the ATR evaluation, combustion could be modeled to include its turbulent effects.

The viscosity model uses approximations that may not entirely be accurate. Precise viscosity model accounting for polar nature of steam and small molecular size of hydrogen could improve the results. Finally, there is a possibility of incorporating the 1-D model in a 2-D grid, such as honey comb structure which could lead to better design and thermal management

REFERENCES

[1] 11 October 2010; Available at: http://en.wikipedia.org/wiki/Albert_Bartlett.

[2] World Population Growth. Available at: http://www.susps.org/overview/numbers.html.

[3] Resource Consumption. Available at: www.asponews.org.

[4] Campbell C. The Association for the Study of Peak Oil. Available at: http://www.peakoil.net/.

[5] Hubbert Curve. Available at: www.lifeaftertheoilcrash.net.

[6] U. Bardi, Energy, 34 (2009) 323-326.

[7] http://www.eia.doe.gov/cneaf/electricity/epa/figes1.html,.

[8] Available at: http://ecohearth.com/eco-zine/green-issues/401-the-dangers-of-coal-burning-power-plants-.html.

[9] A.P. Lanz, J. Heffel, C. Messer, Revision 0 (2001).

[10] J.R. Rostrup-Nielsen, J. Sehested, J.K. Norskov, Advanced Catalysis, 47 (2002) 65-139.

[11] P.K. Cheekatamarala, A.M. Lane, Journal of Power Sources, 152 (2005) 256-263.

[12] K.S. Patel, A.K. Sunol, Journal of Power Sources, 161 (2006) 503-512.

[13] T. Giroux, S. Hwang, Y. Liu, W. Ruettinger, L. Shore, Applied Catalysis B: Environmental, 56 (2005) 95-110.

[14] A.M. De Groote, G.F. Froment, Applied Catalysis A: General, 138 (1996) 245-264.

[15] P.K. Cheekatamarala, The Department of Chemical and Biological Engineering, The University of Alabama, (2004).

[16] Z. Chen, Y. Yan, S. El-Nashaie, Chemical Engineering Science, 58 (2003) 4335-4349.

[17] P.V. Beurden, ECN-I--04-003 (2004).

[18] D. Li, T. Shishido, Y. Oumi, T. Sano, K. Takehira, Applied Catalysis A: General, 332 (2007) 98-109.

[19] L. Zhou, Y. Guo, Q. Zhang, M. Yagi, H. Li, J. Chen, M. Sakurai, H. Kameyama, Catalysis Communications, 10 (2008) 325-329.

[20] Y. Zhan, D. Li, K. Nishida, T. Shishido, Y. Oumi, T. Sano, K. Takehira, Applied Clay Science, 45 (2009) 147-154.

[21] K. Hou, R. Hughes, Chemical Engineering Journal, 82 (2001) 311-328.

[22] I.M. Bodrov, L.O. Apel'baum, M. Temkin, Kinet. Catal., 5 (1964) 696-704.

[23] A.A. Khomenko, L.O. Apel'baum, F.S. Shub, Y.S. Snagorskii, M. Temkin, Kinet. Catal., 12 (1971) 367.

[24] J. Xu, G.F. Froment, AIChE. Journal, 35 (1989).

[25] J. Wei, E. Iglesia, Journal of Catalysis, 225 (2004) 116-127.

[26] D. Mogensen, J.D. Grunwaldt, P.V. Hendriksen, K. Dam-Johansen, J.U. Nielsen, Journal of Power Sources, doi:10.1016/j/jpowsour.2010.06.091 (2010).

[27] J. Yuan, X. Lv, B. Sunden, D. Yue, International Journal of Hydrogen Energy, 32 (2007) 3887-3898.

[28] M.E.E. Abashar, International Journal of Hydrogen Energy, 29 (2004) 799-808.

[29] D. Papadias, S.H.D. Lee, D.J. Chmielewski, Industrial and Engineering Chemistry Research, 45 (2006) 5841-5858.

[30] E.L.G. Oliveira, C.A. Grande, A.E. Rodrigues, Chemical Engineering Science, 65 (2010) 1539-1550.

[31] H. Zhang, L. Wang, S. Weng, M. Su, Journal of Power Sources, 183 (2008) 282-294.

[32] K.W. Whitten, R.E. Davis, M.L. Peck, General Chemistry, Seventh Edition ed., Brooks/Cole; 2004.

[33] B.R. Bird, W.E. Stewart, E.N. Lightfoot, Transport Phenomena, Second Edition ed., John Wiley & Sons, pp. 27-29; 275-278.

[34] D.L. Hoang, S.H. Chan, Applied Catalysis A: General, 268 (2004) 207-216.

[35] J. Pasel, J. Meißner, Z. Porš, R. Samsun, A. Tschauder, R. Peters, International Journal of Hydrogen Energy, 32 (2007) 4847-4858.

[36] S. Roychoudhury, M. Lyubovsky, D. Walsh, D. Chu, E. Kallio, Journal of Power Sources, 160 (2006) 510-513.

[37] A. Mahecha-Botero, T. Boyd, A. Gulamhusein, N. Comyn, C.J. Lim, J.R. Grace, Y. Shirasaki, I. Yasuda, Chem. Eng. Sci., 63 (2008) 2752-2762.

[38] M. Sommer, A. Lamm, A. Docter, D. Agar, Journal of Power Sources, 127 (2004) 313-318.

[39] M.H. Halabi, M.H.J.M. de Croon, J.V.D. Schaaf, P.D. Cobden, J.C. Schouten, Chemical Engineering Journal, 137 (2008) 568-578.

[40] J. Huppmeier, S. Barg, M. Baune, D. Koch, G. Grathwohl, J. Thoming, Fuel, 89 (2010) 1257-1264.

[41] Y.A. Cengel, M.A. Boles, Thermodynamics, Sixth Edition, Tata McGraw-Hill; 2008, pp.881.

BIOGRAPHICAL INFORMATION

Srikanth Honavara-Prasad was born in Bangalore, India, in August 1987. He completed his Bachelor's in Mechanical Engineering from the Visveswaraya Technological University, India, in 2008. He then joined The University of Texas at Arlington to pursue his MS in Mechanical Engineering. He worked with Professor Dr. Daejong Kim at the Microturbomachinery and Energy Systems Laboratory, as a research assistant and specialized in the area of Hydrogen production from reforming of hydrocarbons. During the course of his research he developed computational models for steam and auto-thermal reforming. He also developed a computational model to integrate a fuel reformer with a solid oxide fuel cell using the principle of anode recirculation as part of a graduate project. In October 2010, he attended the Fuel Cell Seminar and Exposition at San Antonio, Texas and presented a poster regarding steam reforming. His research interests include energy from all forms of renewable sources.